Laboratori Nazionali di Frascati

LNF-89/073(P)
2 Novembre 1989

A Bianconi, A. Marcelli:

SURFACE XANES

Published on
"Synchrotron Radiation Research: Advances in Surface Science"
Part I, Chapt. A2 , Edited by R.Z. Bachrach
Plenum Publishing Corporation, New York,

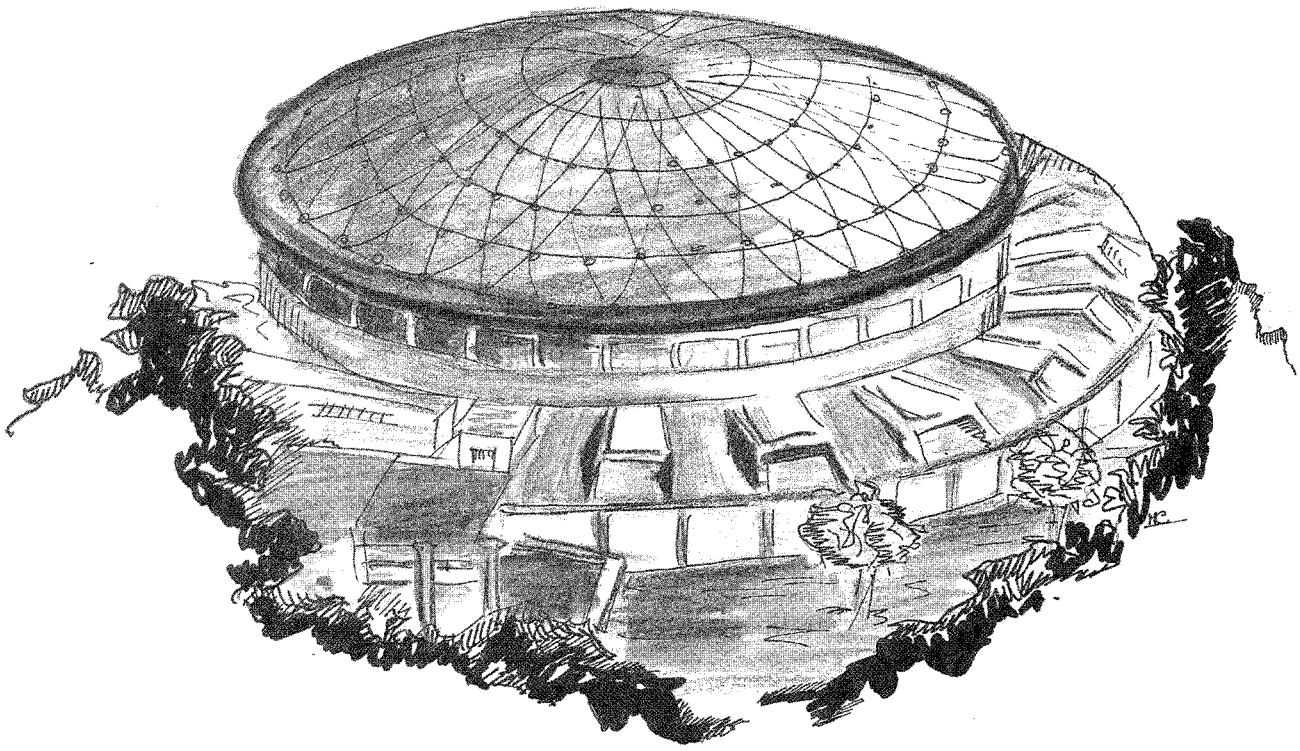

Servizio Documentazione
dei Laboratori Nazionali di Frascati
P.O. Box, 13 - 00044 Frascati (Italy)

INFN - Laboratori Nazionali di Frascati
Servizio Documentazione

LNF-89/073(P)
2 Novembre 1989

SURFACE XANES

A Bianconi
Gruppo Nazionale di Struttura della Materia e Centro Interuniversitario di Struttura della Materia, Dipartimento di Fisica, Università di Roma "La Sapienza", 00185 Roma - Italy

A. Marcelli
INFN - Laboratori Nazionali di Frascati, P.O. Box 13, 00044 Frascati - Italy

TABLE OF CONTENTS

Abstract

The x-ray absorption near edge structure (XANES) in the surface x-ray absorption spectra is discussed. The XANES is interpreted in the real space in the framework of the multiple scattering theory. A review of some applications of surface XANES to the study of clean surfaces, of atomic and molecular chemisorption and of surface oxidation is given.

1. - Introduction

Surface x-ray absorption spectroscopy concerns the study of electronic transitions from core levels of atoms at the surface of solids. The local character of core level excitations makes attractive the study of atoms at the surface of solids to investigate both the local structure and the localized electronic states. Moreover the large energy separation between different inner shells makes possible to select a particular core level of a selected atomic species.

The knowledge of atomic arrangement of neighbor atoms around a selected atom on a surface is important for example in the study of chemisorption and oxidation processes. In fact the local structure of chemisorption sites and the local structure of surface amorphous oxides are basic information not directly given by other techniques based on diffraction methods like Low Energy Electron Diffraction (LEED).(1)

Surface x-ray absorption spectroscopy was born in the middle of seventies when tunable x-ray synchrotron radiation emitted by intense and stable sources, electron storage rings, become available. The requirements for the x-ray source was the tunability to carry out spectroscopy measurements and the high intensity because of the low concentration of surface atoms.

The main experimental problem to be solved was to find experimental techniques with high surface sensitivity. Lukirskii and Brytov in 1964(2) using the continuum bremsstrahlung of a standard soft x-ray tube and later Gudat and Kunz in 1972,(3) using synchrotron radiation, demonstrated that the total electron yield (TY) by the sample surface is proportional to the bulk absorption coefficient. The sampling depth of this technique is of the order of magnitude of hundreds angströms (Å) making this technique suitable for bulk investigations.

The first experiment of surface x-ray absorption with high surface sensitivity was carried out in 1977 at the Stanford synchrotron radiation facility by Bianconi, Bachrach and Flodstrom(4) by detection of the Auger electron yield. The absorption spectrum of the Al surface atoms in the top monolayer of an aluminum crystal was distinguished from the aluminum bulk spectrum. (see Figure 1). The surface contrast was increased by selecting an Auger line due to Al surface atoms interacting with chemisorbed oxygen (an inter-atomic, aluminum-oxygen Auger transition).

The theoretical relation between Auger electron yield and surface absorption coefficient was independently predicted by Lee(5) and Landman and Adams.(6) Both the total electron yield(7) and the Auger electron yield(8) methods were used to measure the Surface Extended X-ray Absorption Fine Structure (SEXAFS) of different atomic species chemisorbed on solids but the absorption coefficient of the atoms on the clean surface can be detected only selecting an Auger line of the order of ~50 eV which corresponds to the minimum in the curve of the electron escape depth.(9)

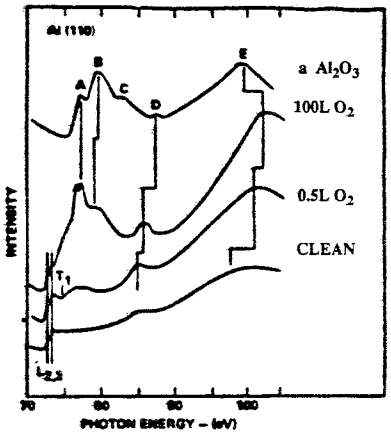

FIG. 1 - Aluminum $L_{2,3}$ surface XANES of Al ions at the Al(110) surface interacting with 100 L of chemisorbed oxygen (1L=10^{-6} Torr x 1 sec) corresponding to about one monolayer coverage detected by Auger Al(2p)O(2s)V (E_f= 45.5 eV) electron yield. The lowest curve shows the minor contribution of the Al metal substrate (clean spectrum). The upper curve shows the Al L_{23} XANES of bulk amorphous Al_2O_3. The differences betweeen the XANES curve (100L O_2) of Al interacting with chemisorbed oxygen and that of bulk oxide (a-Al_2O_3) shows the specific Al-O coordination in the chemisorbed phase.(4)

SEXAFS concerns the study of the modulation of the absorption coefficient over a range of photoelectron wavevector above about 3 $Å^{-1}$. In these range experimental data can be analyzed in the framework of the EXAFS theory.(10) Several reviews about SEXAFS has been published in these years.(11-16)

The structures in the low energy range of few tens of electron volt of the x-ray absorption spectra in the range called X-ray Absorption Near Edge Structure (XANES),(11,14) has attracted interest because it contains information on the local geometry i.e. both on bond distances and on bond angles. In fact higher order terms of the correlation function of the atomic distribution become important in the XANES energy region while only the pair correlation function of the atomic distribution gives the main contribution in the EXAFS range.

In the early surface XANES experiments the application of XANES for local geometry determination has been limited to a fingerprint approach using model compounds(17,18) due to the lack of reliable theoretical analysis. In these last years important advances towards quantitative theoretical analysis of the XANES data have been carried out.

In section 2 an overview of theoretical XANES calculations will be presented. Section 3 gives a brief panorama over the experimental methods while the last section 4 reviews some applications of surface XANES.

2. - Calculation of XANES

X-ray absorption near edge structure concerns the electronic transitions from atomic inner shells to unoccupied states. In the classical quantum theory the absorption cross section is given by many-body excitations of the N-electron system. Following the interaction with

final state f at energy E_f. In the dipole approximation the total absorption cross section is given by

$$\sigma(\omega) \sim \omega \sum_f |M_{if}|^2 \delta(E_i - E_f + \omega) \qquad (1)$$

where the sum is extended over all the possible final states f and M_{if} is the matrix element involving the initial Ψ_i and final Ψ_f^* many-body radial wave functions

$$M_{if} = \int \Psi_f^*(r_1, r_2, \ldots, r_n) \sum_n (\mathbf{r}_n \cdot \mathbf{e}) \Psi_i(r_1, r_2, \ldots, r_n)\, dr \qquad (2)$$

where $\mathbf{e}$ is the unitary polarization vector of the electric field and the $\mathbf{r}_n$ is the vector describing the position of the n-th electron.

In the one-electron approximation the x-ray absorption is described by single-particle processes. The N-electron system is separated into two parts: the single electron in the core level which is excited into an unoccupied level and the N-1 passive electrons which do not participate directly in the electronic transition. The one-electron transition takes place in a static potential determined by a single configuration of the N-1 passive electrons.

In the case of metals, the core hole in the static final state potential is fully screened by valence electrons close to the Fermi level. Most of the XANES spectra can be interpreted in the frame of the von Barth and Grossmann final state rule,[19,20] which states that the wave function of the excited photoelectron is determined by the final state potential with the core hole and the relaxed N-1 electrons. Therefore in most cases the one-electron transitions are assumed to take place in the potential of the fully relaxed configuration of the N-1 passive electrons in the presence of the core hole. The fully relaxed configuration is defined as the final state many-body configuration with the lowest energy. The final state rule breaks down for transitions to nearly filled bands like in the case of $2p \rightarrow \varepsilon d$ transition in palladium or in nickel metal.

Many-body effects can arise because of the presence of different many-body final state configurations of the N-1 passive electrons. Configuration interaction of many-body final states can appear because of core hole perturbation in the final state and/or configuration interaction in the ground state like in valence fluctuating materials.[21]

2.1. - The band structure approach

The absorption coefficient $\mu_c(E)$ for the transitions from the core level $c(n,\ell,J)$ with energy E_c and wavefunction φ_{cM}, in the one-electron approximation, can be expressed in atomic units as

where α^{-1}=137.036 is the inverse fine-structure costant, Ω is the volume of the primitive cell, ν is the number of contributing atoms in the primitive cell and $F_c(E)$ is the spectral distribution of oscillator strength[22]

$$F_c(E)= (\omega/3) \sum_{k,j} \sum_{M=-J} r^2_{cM,kj} \delta(E - E_{kj}) \quad (4)$$

$$r_{cM,kj} = \int \varphi_{cM}(r)\, r\, \Psi_{kj}(r)\, d^3r = \langle \varphi_{cM} | r | \Psi_{kj} \rangle \quad (5)$$

Ψ_{kj} and E_{kj} are the wavefunction and energy of the j-th conduction band at reduced vector $\mathbf{k}$, ω is the photon energy $\omega = E - E_c$ and the integration is carried out over the volume of the primitive cell. Since the dipole transitions dominate the process of photoabsorption, an electron from a core level having angular momentum ℓ is excited into the $\ell\pm1$ final states. Neglecting the spin-orbit coupling for the band states, $F_c(E)$ can be written as[23,24]

$$F_c(E) = (\omega/3)\, (2J+1)/(2(2\ell+1)\, \{ \ell/(2\ell-1) f_{c,\ell-1}(E) + (\ell+1)/(2\ell+1)\, f_{c,\ell+1}(E)\} \quad (6)$$

where the partial strength $f_{c,\ell}(E)$ can be factorized into

$$f_{c,\ell}(E) = \rho_{c,\ell}\ N_\ell(E) \quad (7)$$

$N_\ell(E)$ is the angular projected density of states defined as

$$N_\ell(E) = 2 \sum_{k,j} \sum_m |\langle Y_{\ell m} | \Psi_{kj} \rangle|^2\, \delta(E - E_{kj}) \quad (8)$$

where the energy band states are labelled by the reduced wave vector $\mathbf{k}$ and the band index j. The effective matrix element $\rho_{c,\ell}(E)$ is given by

$$\rho_{c,\ell}(E) = \langle \varphi_c | r | \phi_\ell(E) \rangle^2 / \langle \phi_\ell^2(E) \rangle \quad (9)$$

where the wave function $\phi_\ell(E,r)$ is a solution of the radial Schrödinger equation inside the muffin-tin (MT) sphere of radius S (r<S), and outside the MT sphere (r≥S), is given by

$$\phi_\ell(E,r) = [\cos \delta_\ell(E)]\, J_\ell [(E-V_O)^{1/2} r] - [\sin \delta_\ell(E)]\, n_\ell [(E-V_O)^{1/2} r] \quad (10)$$

where $\delta_\ell(E)$ is the ℓ-th phase shift of the muffin tin potential, V_O is the muffin tin zero of the potential and J_ℓ and n_ℓ are spherical Bessel functions.

The spectra of crystals are therefore interpreted in terms of the product of the partial (of selected orbital momentum $\ell\pm1$) density of states and of the matrix element. Theoretical calculations of the partial and projected density of states of the crystal band structure were

reported by several authors to interpret the XANES spectra.[25-33] In Figure 2 the large differences between the K-edge and the L_3 edge of Si crystal are interpreted as arising from the difference between the $\ell=0$ and the $\ell=1$ partial density of unoccupied states of the conduction band.[33]

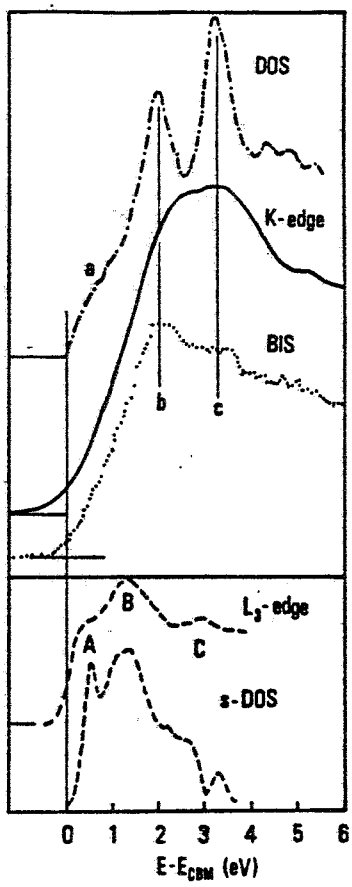

FIG. 2 - Si K-edge and Si L_3 edge absorption spectra. The Si L_3 is compared with the partial (l=0) s density of states of the unoccupied conduction band, lower panel. The Si K-edge spectrum is compared with the total density of states (mostly p (l=1)). The BIS spectrum, which is often assumed to probe the total density of states is shown for comparison.[33]

Müller et al.[23,24] have shown that the XANES spectra can be understood as the product of an atomic-like term and a solid state term. The factorization of the partial oscillator strength into the solid state term $\chi_\ell(E)$ and atomic term $f^{at}_{c,\ell}(E)$ is given by

$$f_{c,\ell}(E) = f^{at}_{c,\ell}(E)\,\chi_\ell(E). \qquad (11)$$

The atomic term is obtained by considering a single muffin tin potential confined in the Wigner-Seitz (WS) sphere of radius S_{WS} and the spectrum for the transition from the core level in the single atom is

$$f^{at}_{c,\ell}(E) = (2\ell+1)\,N^{FE}(E) < \varphi_c \mid r \mid \phi_\ell(E,r) >^2 \qquad (12)$$

where the integration is over the Wigner-Seitz (WS) sphere and $N^{FE}(E) = (E - V_o)^2/2\pi$ is the free electron density of states. The solid state term is

$$\chi_\ell(E) = N_\ell(E) / N^{at}_{c,\ell}(E) \qquad (13)$$

where

$$N^{at}_{c,\ell}(E) = 1/\Omega\,(2\ell+1) N^{FE}(E) < \phi_\ell^2(E,r) > \qquad (14)$$

is the projected density of states for the single-sphere problem.

This approach leads to the following understanding of the of the x-ray absorption spectra: i) the overall magnitude and shape of a particular spectrum is determined by the corresponding atomic transition rate $f^{at}_{c,\ell}(E)$ and ii) the fine structure of the spectrum is determined by the solid state factor $\chi_\ell(E)$ which is proportional to the density of band states with $\ell\pm1$ orbital characters.

The ℓ-1 term is often ignored because usually it exhibits a much smaller amplitude than the ℓ+1 term. However in some cases, like in the first six electron volt above theshold in the Si L_3-edge, the ℓ+1 density of states is negligible and the ℓ-1 term is the most important.

In some cases the atomic part exhibits strong resonances in a small energy range therefore the contribution of the solid state factor $\chi_\ell(E)$ can be neglected. In these cases the spectra of solids can be interpreted in terms of atomic transitions (see for examples the $L_{2,3}$ edges of Ni and Cu in insulating systems).[34,36] In other cases the atomic part exhibits a smooth structureless spectrum over a large energy range and therefore the spectral features can be assigned to the solid state factor $\chi_\ell(E)$.

It is very important to include in the theory the lifetime of the photoelectron in order to get a good agreement between calculated spectra and experiments. The lifetime of the photoelectron takes account of the inelastic scattering of the photoelectron with valence electrons which is an essential physical aspect of the states at high energy in the conduction band because the photoelectrons with energy E have enough energy to excite all valence electrons with binding energy smaller than E.

2. 2. - The multiple scattering approach

Experimental evidence that the K-edge XANES of several systems over a range of about 50 eV depend mainly on the geometrical structure of a finite cluster of atoms around the absorbing atom was found.[11,37,38] An interpretation of the x-ray absorption near edge structure in terms of multiple scattering resonances of the photoelectron in a cluster of finite size in the real space was proposed. This interpretation was based on an extention to condensed systems of the shape resonances which are localized states in the continuum, in the spectra of diatomic molecules like N_2,[39] which were interpreted with a multiple scattering theory by Dill and Dehmer.[40]

The size of the cluster relevant for XANES was found to change in different systems ranging from a single shell to several shells around a photoabsorbing atom depending on the electron mean free path for inelastic scattering and on the core hole lifetime in crystalline solids. In disordered systems (i.e. amorphous and liquid systems) the structural disorder reduces the number of neighbour shells to one or two.

The comparison between the calculated absorption coefficient and the experiments indicates that the theoretical spectra have to be convoluted with an intrinsic Lorentzian

agreement. The intrinsic broadening of the excited states $\Gamma(E)$ is the sum of two terms: the first is the core hole width Γ_h and the second term is the energy band width $\Gamma_e(E)$ of the excited electron of energy E. These are related to τ_h the core hole lifetime and to $\tau_e(E)$ the lifetime of the electron, which is a function of the mean free path of the excited electrons $\lambda(E)$. $\lambda(E)$ is determined by the inelastic scattering of the photoelectron with the passive electrons, it is energy dependent and varies for each material:

$$\Gamma_{tot}(E) = \Gamma_h + \Gamma_e(E) = (h/2\pi)/\tau_h + (h/2\pi)/\tau_e(E) = (h/2\pi)\,[1/\tau_h + 2(2E/m)^{1/2}/\lambda(E)] \tag{15}$$

At low kinetic energies of the electron $\Gamma_h > \Gamma_e$ and the Γ_h term dominates while at high energies $\Gamma_h < \Gamma_e$, therefore the $\Gamma_e(E)$ term dominates. It is possible to define an effective mean free path given by

$$\lambda_{eff}(E) = (h/2\pi)\,2(2E/m)^{1/2} / \Gamma_{tot}(E). \tag{16}$$

In Figure 3 the mean free path $\lambda(E)$ in a silicon crystal obtained by photoelectron escape depth measurements, the derived $\Gamma_e(E)$, and the $\lambda_{eff}(E)$ using Γ_h=0.4 eV for the Si K-level width, are plotted. λ_{eff} is an extimation of the radius of the cluster probed by XANES. In recent years several theoretical approaches have been developed to solve the absorption cross section for core transitions in real space in the frame of multiple scattering theory.(40-53)

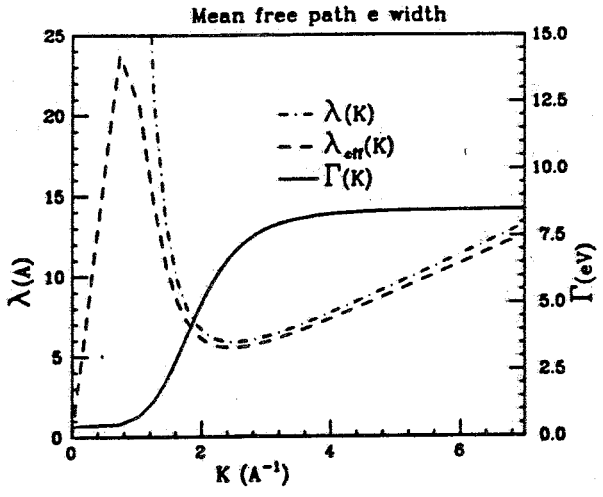

The generally strong scattering power of the atoms of the medium for low kinetic energy photoelectrons favours multiple scattering (MS) processes. At higher energies such that the atomic scattering power becomes small a single scattering (SS) regime is found. In a SS regime the modulation in the absorption coefficient is substantially due to interference of the outgoing photoelectron wave from the absorbing atom with the backscattered wave from each surrounding atom, giving the extended x-ray absorption fine structure (EXAFS).[54,55] Hence EXAFS provides information about the pair correlation function. By decreasing the photoelectron kinetic energy a gradual transformation occurs from the EXAFS regime to the XANES regime.[56-59]

Therefore the EXAFS part probes the first-order or pair correlation function of the atomic distribution near the absorbing atom, while XANES probes the triplet and the higher orders of the atomic distribution function. Interest in determination of higher order correlation functions of local atomic distributions in complex systems has stimulated the growth of XANES.

Multiple-scattering theories have been used in recent years to solve the XANES spectra of crystals, amorphous solids, surfaces, biological molecules, liquids, catalysts and chemical compounds.[60-77] The multiple scattering method has been developed in nuclear physics to calculate nuclear scattering cross sections and in solid state physics to compute the electronic structure of solids. The extension of the bound state molecular scattering method of Johnson and co-workers[78] to determine the one-electron wave function for continuum states was formulated first by Dill and Dehmer.[40] The continuum wave function is matched to the proper asymptotic solution of the Coulomb scattering states, in this way the multiple scattering problem is changed from an homogeneous eigenvalue problem (bound states) to an inhomogeneous one in which the continuum wave function is determined by an asymptotic T-matrix normalization condition.[42] In this scheme the total potential is represented by a cluster of nonoverlapping spherical potentials centered on the atomic sites and the molecule as a whole is enveloped by an "outer sphere". Three regions can be identified in this partitioning: atomic regions (spheres centered upon nuclei, normally called region I); extramolecular region (the space beyond the outer sphere radius, region III) and an interstitial region of complicated geometry in which the molecular potential is approximated by a constant "muffin tin" potential. The Coulomb and exchange part of the input potential are calculated on the basis of a total charge density obtained by superimposing the atomic charge densities, calculated from Clementi and Roetti tables,[79] of the individual atoms constituting the cluster. For the exchange potential it is possible to use both the usual energy independent Slater approximation[80] and the energy-dependent Hedin-Lundqvist[81] potential in order to incorporate the dynamical effect. Following this theory, the expression for absorption coefficient for a cluster of atoms, for polarized light in the vector e direction, is given, in the dipole approximation by

$$\mu_C(E) = N_C\, \sigma(E,e) = N_C\, \sigma(k,e) \qquad (17)$$

$$\sigma(k,e) = 4\pi\omega\, \alpha\, k\, \mathbf{Im}\, [\, \Sigma_{L,L'} \langle \varphi_C \mid r \cdot e \mid \phi_{\ell} Y_L \rangle\, \tau_{L,L'} \langle \phi_{\ell'} Y_{L'} \mid r \cdot e \mid \varphi_C \rangle] \qquad (18)$$

where $\sigma(E,e)$ is the photoabsorbing cross section, N_C is the density of atoms, $L=(\ell,m)$ is the angular momentum, α is the fine structure constant, k is the photoelectron wave number and the spin dependence has been neglected. ϕ_{ℓ}'s are regular solutions of the radial Schrödinger equations in the photoabsorber muffin-tin sphere matching the same boundary conditions as in the equation 10.[82-84] All the structural information are contained in the quantity

$$\tau_{L,L'} = (\, \sin \delta_{\ell}(E) \sin \delta_{\ell'}(E)\,)^{-1}\, [(\, \mathbb{T}_a^{-1} - \mathbb{G})^{-1}]_{L,L'} \qquad (19)$$

where δ_{ℓ}^{ρ} is the ℓ-th phase shift of the absorbing atom assumed located at site 0, $\mathbb{G}=G_{L,L'}$ is the matrix describing the free spherical wave propagation of the photoelectron from site i and angular momentum $L=(\ell,m)$ to site j and angular momentum $L'=(\ell',m')$ in the angular momentum representation and $\mathbb{T}_a = \delta_{i,j}\, \delta_{L,L'}\, [\exp(i\, \delta_{\ell}^{i})\, \sin \delta_{\ell}^{i}]$ is the diagonal matrix of atomic t-matrix elements describing the scattering process of the L spherical wave photoelectron by the atom located at site i with phase shift δ_{ℓ}^{i}. Under certain conditions[56-59] it is possible to express the structural factor as an absolute convergent series and to expand the photoabsorption cross section in partial contributions as following

$$\sigma(E,e) = \Sigma_{n=0}\, \sigma_n(E,e) \qquad (20)$$

The n=0 term represents the smoothly varying "atomic" cross section, the n=1 term is always zero and the generical term n is the contribution to the photoabsorption cross section that comes from processes in which the photoelectron has been scattered n-1 times by the surrounding atoms before returning to the photoabsorbing site. In particular the $\sigma_2(E,e)$, the EXAFS term in the spherical wave representation can be written both for the K edge and L_1 edge as an approximation to the general polarized EXAFS formula[85]

$$\sigma_2(E,e) = |M_{01}(E)|^2 (-1)\, \Sigma_j \cos^2\theta_j\, \mathbf{Im}\{ \exp(2i(\rho_j + \delta_{\ell}^{\rho}))/\rho_j^2)\, \Sigma_{\ell} (-1)^{\ell} (2\ell+1) t_{\ell}^{j}\, f_{\ell}^{2}(\rho_j) \} \qquad (21)$$

where $\rho_j = kR_j$, θ_j is the angle between the polarization vector e and the direction R_j joining the j-th atom with the absorbing one, $|M_{01}(E)|^2$ is the radial matrix element between the initial $\ell=0$ state and the final dipole allowed R_1 radial wavefunction and the quantity f_{ℓ} which takes into account the spherical correction to the free propagators.[84,85] The total absorption coefficient can be written as

$$\mu(E,e) = \mu_0\, [\, 1 + \Sigma_{n\geq 2}\, \chi_n(E,e)\,] \qquad (22)$$

here $\mu_o(E)$ is the structureless absorption coefficient of a central photoabsorbing atom and $\chi_n(E)$ represents the contribution arising from all MS pathways beginning and ending at the central atom and involving n-1 neighboring atoms. A pictorial view of the multiple scattering pathways contributing to the XANES is shown in Figure 4.

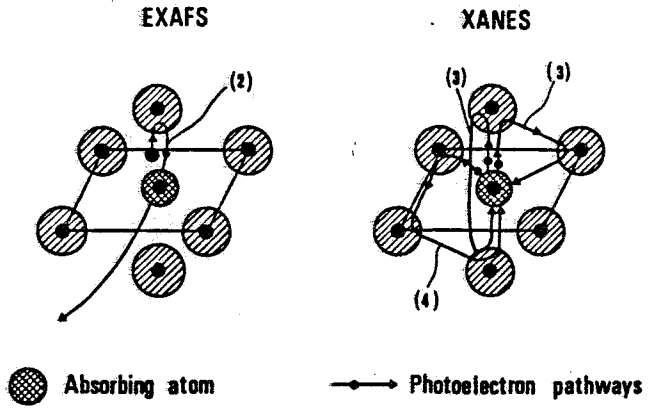

FIG. 4 - Pictorial view of the single scattering process of the excited photoelectron giving the EXAFS signal $\chi_2(E)$ and the multiple scattering processes giving $\chi_3(E)$ and $\chi_4(E)$ contributions.

The terms χ_n are usually plotted versus the wave vector, k, of the photoelectron. The EXAFS $\chi_2(k)$ term is the dominant term above wave vector values k> 3~4 $Å^{-1}$. The $\chi_3(k)$ term is the double scattering signal arising from all the triangular paths with one vertex on the central atom. The multiple scattering signal is defined as

$$\chi_{MS}(k) = \Sigma_{n\geq 2}\chi_n(k) = ([\,\mu(k) - \mu_o(k)\,] / \mu_o(k)) - \chi_2(k) \qquad (23)$$

The general mathematical expression for $\chi_n(k)$, without taking into account the inelastic interactions of the photoelectron, i.e. its mean free path and the structural Debye-Waller factor, can be written as

$$\chi_n{}^{\ell}(k) = \Sigma p_n\, A_n{}^{\ell}(k,p_n) \sin (kR p_n + \phi_n{}^{\ell}(k,p_n) + 2\delta_{\ell}{}^{o}) \qquad (24)$$

where $\delta_{\ell}{}^{o}$ is the central atom ℓ-th phase shift and the dependence of the amplitude and phase function $A_n{}^{\ell}$ and $\phi_n{}^{\ell}$ on the particular path has been indicated symbolically by p_n. General expressions for calculating the quantities $A_n{}^{\ell}$ and $\phi_n{}^{\ell}$ in terms of the atomic phase shifts and the geometry of the path p_n are provided by the MS theory. A substantial simplification of

propagator of the photoelectron in the final state, the spherical-wave approximation (SWA),(86) which preserves the spherical wave character of the propagation and is rather accurate even at very low wave vector values (k≈1-2 Å^{-1}).

Due to the general structure of the quantities $\chi_n{}^{\ell}(k)$, the amplitudes $A_n{}^{\ell}$'s decrease with increasing order n, so that usually $\chi_2{}^{\ell}(k)$ is the dominant term in the whole energy range where the series converges. Hence an analysis of the MS contribution beyond the first term is possible if the $\chi_2{}^{\ell}(k)$ contribution is subtracted from the experimental signal: $\chi_{MS}(k)=\chi(k)-\chi_2{}^{\ell}(k)$ provided a good estimate for $\mu_0(k)$ and $\chi_2{}^{\ell}(k)$ is used.

For K-edge neglecting the angular dependence of the Hankel function in the free propagator, the usual EXAFS signal times the atomic part can be obtained for n=2

$$\mu_2 = \mu_0 \chi_2 = \mu_0 \sum_j \mathrm{Im}\ \{\ f_j(k,\pi)\ \exp(2i\delta_1{}^0+kr_j)/kr_j^2\ \} \qquad (25)$$

where r_j is the distance between the central atom and the neighboring atom j and $f_j(k,\pi)$ is the usual backscattering amplitude. The first multiple scattering contribution is the μ_3 term that can be written(84)

$$\mu_3 = \mu_0 \sum_{i\neq j} \mathrm{Im}\ \{\ P_1(\cos\phi) f_i(\omega) f_j(\theta)\ \exp(2i(\delta_1{}^0+kR_{tot}))/kr_i r_{ij} r_j\ \} \qquad (26)$$

here r_{ij} is the distance between atom i and j, $f_i(\omega)$ and $f_j(\theta)$ are the scattering amplitude that now depend on the angles, by Legendre polynomials $P_1(x)$, in the triangle which joins the absorbing atom to the neighbouring atoms located at sites $\mathbf{r}_i$ and $\mathbf{r}_j$ and $R_{tot}=r_i+r_{ij}+r_j$. In this expression $\cos\phi=-\mathbf{r}_i\circ\mathbf{r}_j$, $\cos\omega=-\mathbf{r}_i\circ\mathbf{r}_{ij}$ and $\cos\theta=\mathbf{r}_j\circ\mathbf{r}_{ij}$. So the terms higher than two clearly contains information about the n-th order correlation function. To conclude it is possible to observe that because of $P_1(\cos\phi)=\cos\phi$ there is a selection rule in the pathways that contribute to the μ_3 term, in fact all the cases where $\mathbf{r}_i$ is perpendicular to $\mathbf{r}_j$ do not contribute to this term since $\cos\phi=0$.

2. 3 - A model case: XANES of silicon

Silicon is a particularly good system to test the contribution of MS in the XANES spectra in systems with non collinear paths. In fact considering the absorbing Si atom with seven shells of neighbor atoms with only paths with non collinear configurations. In the case of collinear configurations the high probability for forward scattering enhances MS contributions in the EXAFS,(87,88) while for noncollinear configurations the probability of large angle scattering is very low at high kinetic energies and in fact the EXAFS approximation has been found to work in most of the systems.

The Si K-edge XANES of crystalline silicon measured by KLL Auger yield is reported

shown in the bottom of the Figure is determined by quenching of MS signal and EXAFS contribution of further shells. The multiple scattering effects are important to explain the absorption spectra in the first 70 eV beyond the K threshold giving the peaks A, B and C in the XANES region.(59)

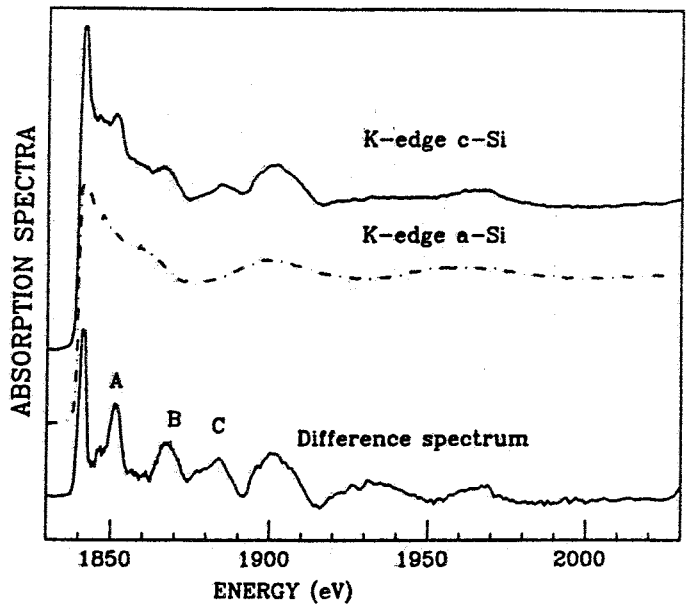

FIG. 5 - X-ray absorption spectra of crystalline (c-Si) and amorphous (a-Si) silicon determined by measuring the intensity of the KLL Auger emission as a function of the photon energy. The lower spectrum shows the difference (α_{cr} - α_{am}) multiplied by 2. The peaks A, B and C are mainly due to the multiple scattering contribution.

The multiple scattering signal was extracted from the experimental spectrum following this procedure. The modulation of the atomic absorption over the high-energy EXAFS and low-energy XANES range was determined by subtracting from the measured spectra a polynomial fitting in order to simulate the smooth atomic absorption contribution $\alpha_0(k)$. The resulting $\chi(k)$ is shown in Figure 6. A good fitting of the EXAFS oscillations in the Si K-edge spectrum from 50 to 450 eV above the absorption threshold was obtained using both the exact spherical wave EXAFS analysis(89) and the spherical wave approximation (SWA). The $\chi_2(k)$ spherical wave signal including the inelastic scattering and the Debye Waller factor has been calculated in the whole energy range above threshold. A good agreement is found between χ_2 and χ in the EXAFS range above about 100 eV from the threshold.

The experimental multiple scattering signal $\chi_{MS}(k)$ has been obtained by subtracting from the experimental oscillatory part $\chi(k)$ of the absorption spectrum the calculated EXAFS

signal $\chi_2(k)$. Following this subtraction procedure over the full experimental energy range, starting from about 5 eV above threshold a very large signal in the first 70 eV above the absorption K-edge that it is not possible to explain by using the single scattering formalism have been found. The result of the subtraction is plotted in Figure 6 (lower curve) and it is compared with the $\chi(k)$ signal (upper curve). Looking at panel A of Figure 6 it is clear that the A, B and C peaks arise mainly from multiple scattering effects.

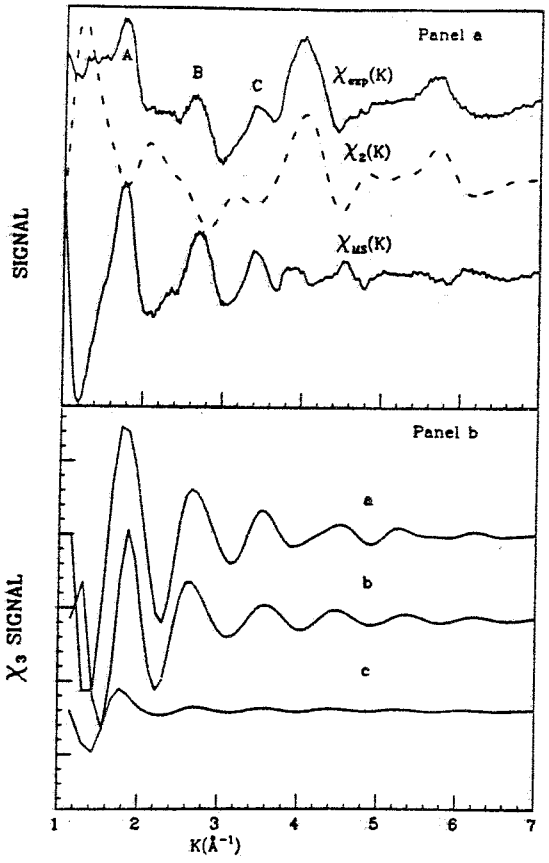

FIG. 6 - (A) Experimental $\chi(k)$ (upper curve) compared with a calculated EXAFS signal $\chi_2(k)$ using the spherical wave formalism (dashed curve) and with the difference spectrum $\chi_{MS}(k)=\chi(k) - \chi_2(k)$ (lower curve). It is important to remark that the A, B and C peaks are mainly due to the multiple scattering contribution.
(B) The upper curve a is the total signal due to all the pathways of double scattering $\chi_3(k)$ within the first three shells which is very close to the experimental χ_{MS} of panel A. The central curve b represents the contribution due to all the pathways with a length of 8.54 Å. As shown, the total χ_3 signal is dominated by the contribution of these shortest paths of double scattering. The curve c is the χ_3 contribution due to paths involving only the first coordination shell around the photoabsorber atom.

Since the first higher order term in the MS series is the $\chi_3(k)$ term a calculation of the contributions arising from the double scattering paths involving two neighbor atoms within the first three shells have been performed introducing the mean free path damping term in the calculation of $\chi_3(k)$. The result (curve **a**) is shown in Figure 6, panel b.

There are 756 paths of double scattering within the first three shells and it is possible to sort them out into 41 groups according to total length and scattering angles relative to the central atom. The groups with low path degeneracy are generally negligible since they give only a weak signal. Moreover has possible to neglect the contribution due to the groups with a very long total length (the perimeter of the triangle) since the mean free path term suppresses their contribution to the spectrum in the energy range beyond 15 eV above the edge, as it has been verified.

The panel B of Figure 6 reports (curve **b**) the damped signal coming from 36 paths with the shortest total length (R_{tot}=8.54 Å). These 36 paths can be divided into two groups differing in the angles θ_o between the outgoing and incoming paths directed at the photoabsorbing vertex. Figure 7 reports a picture of the two classes of shortest double scattering paths where it is stressed the difference in the angles θ_o.

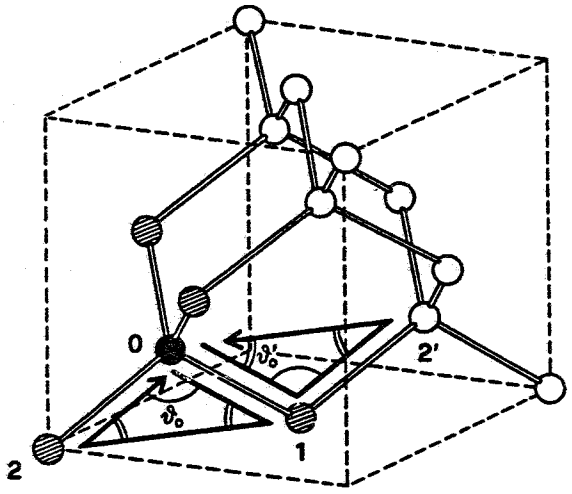

FIG. 7 - Fcc unit cell of the silicon structure. The photoabsorber is the black sphere while are shadowed the first nearest neighbors. Two examples of the 36 shortest double scattering pathways are stressed: the first, 3S1-type, includes the atoms 0, 1 and 2 all within the first coordination shell (there are 12 paths of this type); the second, 3S2-type, includes the atoms 0, 1 and 2' and involves an atom of the second shell (there are 24 paths of this type).

The first of these two groups comprises 12 paths contained within the first neighbour shell. This type of paths, involving the photoabsorbing atom 0 and for example the first shell atoms 1 and 2, are shown in Figure 7 and are classified as 3S1-type paths. Its contribution is

very weak and it is shown by curve **c** in Figure 6B. The second group comprises 24 paths (3S2-type paths) involving the atoms of the second shell (2' atom in Figure 7) and gives the main contribution to the curve **b** shown in Figure 6B. Adding other damped contributions due to the other groups of pathways the χ_3 signal does not change its shape. Therefore the most important contribution to χ_3 comes from the 3S2-type paths with total length of 8.54 Å as it is possible to see by comparing curve **b** with curve **a** in Figure 6B.

The calculated χ_3 is close to the experimental oscillation χ_{MS} as shown in Figure 6A. The differences between χ_{MS} and the theoretical χ_3 can be assigned to higher orders (n>3) multiple scattering contributions.

The difference between the absorption spectra of crystalline and amorphous Si shown in Figure 6 gives experimental evidence for multiple scattering contributions in the XANES of crystalline silicon. The EXAFS difference spectra are determined by the EXAFS contribution of further shells in the crystalline phase but the large peaks in the difference spectrum in the low energy XANES range are mostly determined by the multiple scattering signal which is quenched in the amorphous phase.

3. - Experimental Techniques

This section gives only a brief outline of the experimental aspects of the surface x-ray absorption experiments and the related detection methods.(10)

Synchrotron radiation is required for surface x-ray experiments, indeed the spectral brightness of this source is larger by several order of magnitude over conventional x-ray tubes providing superior signal-to-noise ratio and allowing spectral measurements in very short time with very high resolution. In addition ultra-high vacuum (~10^{-10} Torr) is needed to enable experiment on well characterized surfaces. The experimental set-up for surface x-ray absorption spectroscopy requires special beam lines, dedicated sample chambers and different detection methods depending on several factors:

i) energy of the x-rays involved in the experiment. It is possible to distinguish three energy ranges requiring different types of monochromators: grating monochromators for soft x-rays from 50 to 800 eV, monochromators with crystals with large spacings like beryl ($10\bar{1}0$) and InSb(111) crystals for the range 800-3000 eV, and silicon crystal monochromators for the harder x-ray range (>3000 eV),

ii) concentration of the studied atom on the surface. The low concentration of surface atoms, about 10^{15} atoms cm^{-2} to compare with the bulk concentration (10^{19} atoms cm^{-2}), requires higher x-rays intensities to obtain comparable signal-to-noise ratio,

iii) surface sensitivity, defined as the ratio between the signal due to the surface layer and that due to the substrate. High surface sensitivity can be achieved by limiting the penetration of the incident photon working close to total reflection,(90-92) and by

detecting particles from decay channels of the core hole with the shortest escape length.

The inner shell photoionization process can be described by a two step process at first approximation. In the first step the photon excites a core hole-photoelectron pair and in the second step the recombination process of the core hole takes place. There are many possible channels for the core hole recombination process, these can be of radiative type (fluorescence) producing the emission of photons or nonradiative (Auger transitions) with emission of electrons or ions which can be collected out of the surface with special detectors. Several techniques can be chosen to detect the surface absorption when the selected recombination channel is the electronic decay.(93)

The total electron yield technique (TY) measures the integral over the entire energy range of the electron energy distribution curves (EDC). Comparison of the absorption and electron yield led to the conclusion that the total electron yield signal is proportional to the absorption coefficient.(3) The advantage of this method is that the maximum counting rate is obtained since emitted electrons over a large solid angle can be collected by giving a positive voltage on the detector, on the contrary the surface contrast of this technique is poor because both low energy secondary electrons and high energy photoelectrons are collected.

Similar to the TY is the partial electron yield method (PY) collecting the low-energy secondary electrons within a kinetic energy window around the maximum of the inelastic part of the energy distribution curve (2~4 eV). Selecting only secondary electrons of low kinetic energy the surface sensitivity is similar to the total electron yield.

In the energy range hv<4000 eV the Auger recombination has higher probability than the radiative recombination and the detection of elastically emitted Auger electrons is an efficient way to measure the surface absorption coefficient. The energy of the Auger electrons is characteristic of a particular atom therefore the photoabsorption cross section of a selected atomic species chemiabsorbed on a surface can be measured monitoring the intensity of its characteristic Auger transition as a function of the photon energy. The Auger line is selected by an electron energy analyzer operated in the constant final state mode (CFS) with an energy window of few electron volt. A standard experimental set up for this type of surface x-ray absorption measurements is shown in Figure 8.(11) Auger electron yield (AY) technique offers the largest signal-to-background (adsorbate to substrate) ratio of all electron yield techniques but the smallest signal rate. This tecnique monitoring Auger electrons at kinetic energies in the range 50-100 eV is suitable for the the study of clean surfaces.(9)

The detection of stimulated emission of ions is called photon-stimulated ion desorption (PSID).(94) The ion current due to PSID is proportional to the number of created core holes, i.e. to the photoabsorption cross section of the absorbate. It is a measure of the surface absorption with higher surface contrast in comparison with other detection methods. PSID is a surface sensitive technique since any ions created within the bulk are inevitably re-neutralized on their way on the surface. In addition in principle a great advantage is that

surface structure of an adsorbate complex can be investigated from both the adsorbate as well the substrate side by tuning to the appropriate absorption edge. Unfortunatly different desorption mechanisms and multielectron excitations are present in the ion yield and severely limit the applicability of PSID together with lower count rates obtained with the actual photon flux levels provided by synchrotron radiation. Photon stimulated excitation, in comparison with electron excitation, offers the advantage for surface XANES that the core hole production probability is largest at the threshold of the core excitation.

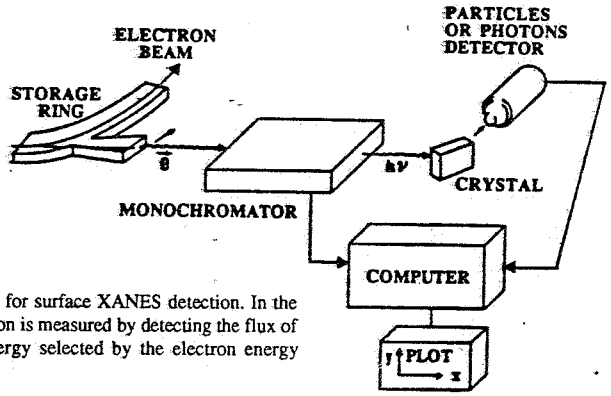

FIG. 8 - Experimental setup for surface XANES detection. In the soft x-ray region the absorption is measured by detecting the flux of the emitted electrons of energy selected by the electron energy analyzer.

In these last years with the development of the first ultra-high vacuum compatible soft x-ray detector for fluorescence photon yield (FY), detection of the XANES above the K edge of light elements has been made possible.(95)

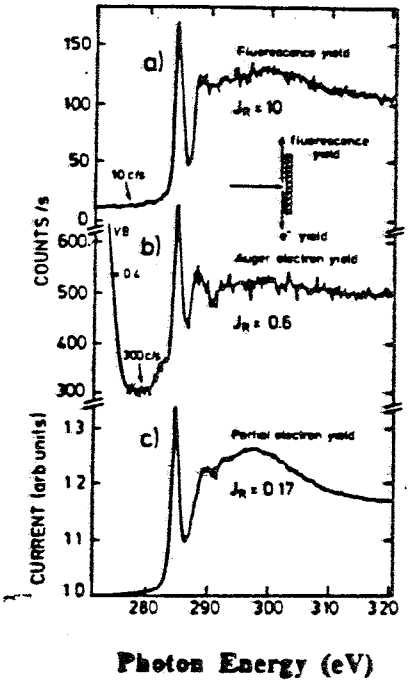

FIG. 9 - Surface x-ray absorption near edge spetra of 10L of C_2H_4 on Cu (100) at 60K (about two monolayers C_2H_4) at normal x-ray incidence recorded with different detection techniques and the detection symmetry axes in the surface plane, along the electric vector e. a) The x-ray fluorescence carbon K_α yield; b) Carbon KVV Auger electron yield; c) Partial electron yield, only electrons with kinetic energy larger than 220 eV were detected. J_R indicates the edge jump or signal/background ratio taken at 320 eV where the near edge features fade out. All the spectra are normalized: covered/clean.(98) with the three electron yield detection modes.

Fluorescence photon yield represents the probability of a core hole in the K or L shell being filled by a radiative process in competition with non radiative Auger recombinations. Due to the small amount of elastically and inelastically scattered backgound from the sample the FY technique gives higher sensitivity. Using soft-x-ray proportional counter an increase more than a factor of twenty in surface sensitivity for chemisorbed monoloyer coverage with comparable signal-to-noise ratio as compared with any conventional electron yield detector was achieved.(95,96) One of the attractive aspects of this technique is the possibility to measure the surface x-ray absorption for in-situ study of the interaction of the surface with gas with a sensitivity better than 1% of monolayer, and also using window valves but with a consistent reduction of flux, from atmospheric pressure up to 10 Torr.(97) Figure 9 shows the surface XANES of chemisorbed C_2H_4 of the surface of Cu(100) at low temperature (T= 60K). The edge jump ratio J_R, which is defined as the count rate difference above and below the edge normalized to the preedge background, is indicated in the figure for the different detection methods. The flurescence photon yield method gives the maximum jump ratio.(98,99)

A new technique to perform surface sensitivity experiments is the XANES in the reflection mode or REFLEXAFS.(92) Since x-rays on entering a substance from the air or the vacuum are going into a medium of smaller refractive index

$$n = 1 - \delta - i\beta \qquad (27)$$

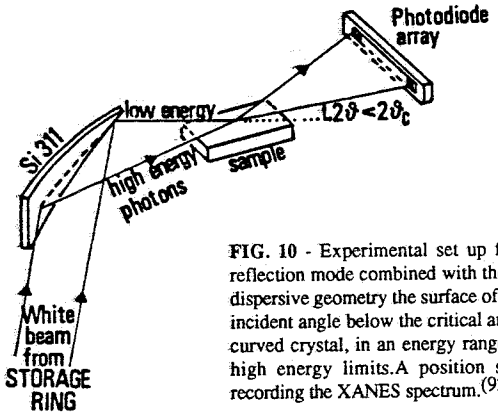

FIG. 10 - Experimental set up for surface absorption in total reflection mode combined with the dispersive x-ray optics. In the dispersive geometry the surface of the sample reflects (for grazing incident angle below the critical angle) photons, diffracted by the curved crystal, in an energy range between the low and and the high energy limits.A position sensitive detector is used for recording the XANES spectrum.(92)

Snell's law indicates that x-rays should be totally reflected from an "optically" plane surface at all glancing angles smaller than the critical angle θ_c given by $\cos\theta_c = (1 - \delta)$ so that $\theta_c \sim \sqrt{2\delta}$. Furthermore, if $\theta < \theta_c$ the incident and reflected beams interfere and give rise to standing waves above the reflecting surface. The electrical field damps out rapidly inside the

material and the penetration depht is almost unrelated to θ, provided $\theta<\theta_c$, and of the order of about 50 Å or less as a function of the material.(100) The great potentiality of this technique in the surface studies can be enhanced by associating the total reflection scheme with the dispersive mode as shown in Figure 10. This approach bears new possibilities for in-situ measurements of the evolution of the surface under various treatments also in non vacuum conditions allowing the study of "real" surfaces moreover it canbe used to investigate either top layers or epilayers.

4. - Applications of Surface XANES

4.1 - XANES of clean surface: Al and Si

The investigation of the structure and electronic states of the surface atoms on the top monolayers of oriented crystals has attracted the interest of a large community in these last years. The measure of surface XANES of a single crystal requires a technique capable to distinguish between surface and bulk atoms of the same atomic species. Surface XANES of clean surfaces has been measured by taking advantage of the short escape depth of low energy Auger electrons with kinetic energy E_f in the range from 30 to 90 eV. Collecting the intensity of low energy Auger electrons of kinetic energy E_f and scanning the photon energy the surface x-ray photoabsorption spectrum with high surface contrast of Al and Si surfaces have been measured. The upper panel of Figure 11 shows the electron energy distribution curve of clean Si(111) 2x1 surface by using photon excitation (hv=130 eV) above the silicon $L_{2,3}$ absorption edge and the inset shows the Si L_3VV Auger signal. In the lower panel the experimental escape depth λ(Å) in silicon for corresponding kinetic energy is shown.

At the photon energy $h\nu=E_0+E_f+\phi$, where the E_0 is the absorption threshold and ϕ is the work function, the kinetic energy of direct core photoelectrons is the same as that of the selected Auger electrons E_f and the core photoelectrons are recorded by the electron analyser giving a spike in the Auger yield spectra. Therefore the surface XANES can be recorded in a limited photon energy range Δ, above the absorption threshold $\Delta = E_f + \phi$. The bulk absorption is simply recorded by changing the final state kinetic energy E_f from the Auger energy to the maximum of the secondary electrons at about 4 eV.

Fig. 12 shows the surface x-ray absorption of Si $L_{2,3}$ edge, of Si(111) 2x1 surface recorded by selecting the LVV Auger electrons at E_f=67 eV compared with the bulk spectrum recorded at E_f=4 eV. The structure in the first 10 eV energy range can be better analysed in terms of band structure approach described in the section 2.1. The variation between the bulk and surface spectra can be assigned to the change of the partial density of states of the conduction band induced by surface reconstruction.(33) The Si (111) 2x1 reconstructed surface following the Pandey model(101,102) gives a different surface partial s-density of states from the bulk. The calculation of the s-partial density of states of the conduction band

for the first few surface monolayers affected by the surface reconstruction gives account for the observed differences between the bulk and the surface absorption (see Figure 13).

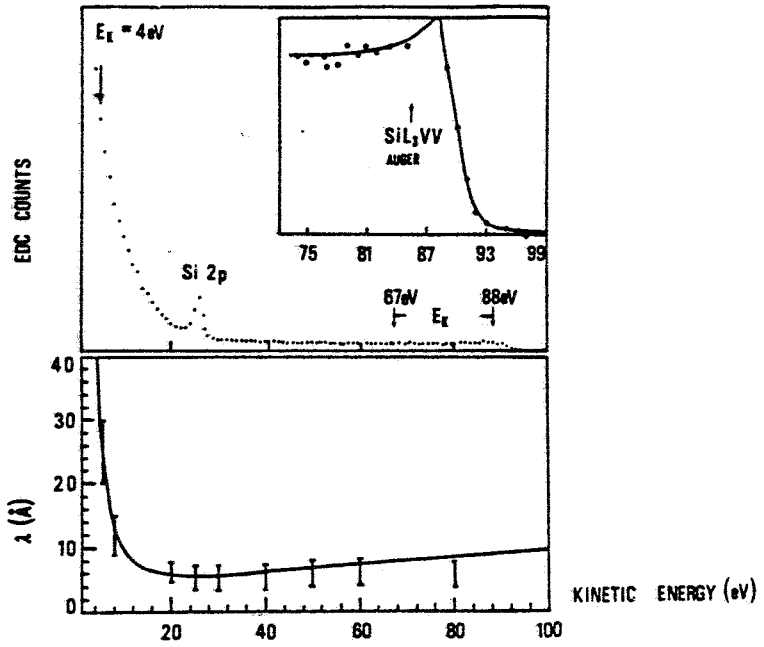

FIG. 11 - Electron energy distribution curve (EDC) of clean Si(111) 2x1 obtained by using photon energy hv=130 eV, upper panel. The inset shows the Si L_3VV Auger signal. In the lower panel the experimental electron escape depth in silicon is shown. The lower panel shows the experimental escape depth λ(E) for emitted electrons of kinetic energy E.

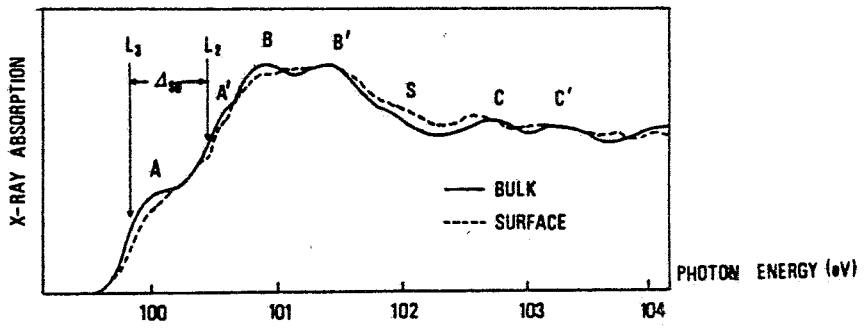

FIG. 12 - Surface (solid line) and bulk (dashed line) $L_{2,3}$ x-ray absorption spectra of a cleaved Si(111) crystal. The bulk spectrum has been recorded by selecting the final state energy of secondary electrons at E_f=4 eV. The surface x-ray absorption spectrum has been recorded by selecting the LVV Auger electrons at E_f=67 eV.

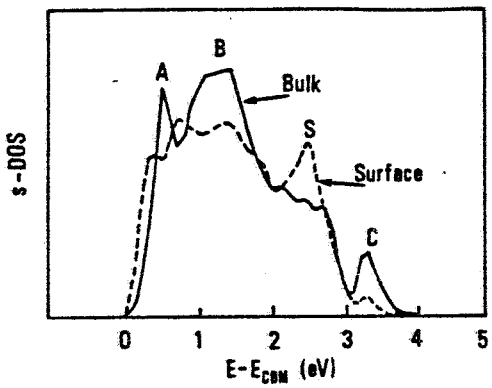

FIG. 13 - Calculated conduction band s density-of-states of bulk silicon (solid line) and of the Si(111) 2x1 surface (dashed line), according to Pandey's π-bonded chain model.

Polarized surface XANES can be recorded using the linear polarization of synchrotron radiation. In Figure 14 the surface XANES at the Si K edge obtained by recording the Si LVV Auger electrons is shown for the two extreme polarization: e//n and e⊥n where **n** is the surface normal vector and **e** is the electric field vector of the radiation. The difference at threshold is due to the unoccupied surface states close to the Fermi energy of p-like character which are observed with the e//n polarization at glancing incidence.[103] According to the discussion in the section 2.3 the features A, B and C are due to higher order multiple scattering contributions and therefore probes the atomic geometrical arrangement. The decrease of the intensity and the change of their shape between normal and glancing incidence is related with the anisotropic structure of the 2x1 reconstructed surface layer.

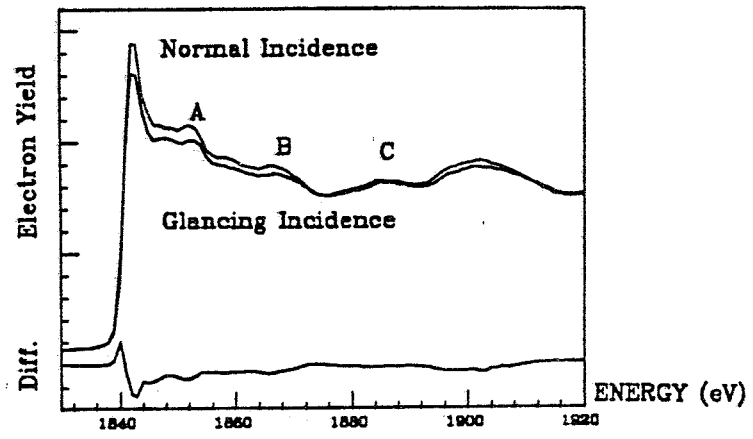

FIG. 14 - Surface silicon K-edge x-ray absorption spectra of the Si(111) 2x1 surface measured by Auger Si LVV electron yield. Upper curve: polarized spectrum at normal incidence (the electric field **e** parallel to the surface plane); lower curve: polarized spectrum at glancing incidence (the electric field **e** nearly perpendicular to the surface plane). The difference curve at the bottom is the diference spectrum between the XANES of the two extreme polarizations.

The clean surface of Si(111) shows large reconstruction of the surface, on the contrary both Al(100) and Al(111) can be considerd as an example of surfaces which do not exhibit surface reconstruction. The main problem of reconstruction concerns the contraction or the expansion of the spacing between the top monolayers. The first few lattice planes of ions at a metal surface can relax inward or outward because the classical Madelung forces tend to drive the first lattice plane sites inward while electronic forces usually tend to drive it outward. The spacing is calculable by direct minimization of surface energy.(104-106) Because the electronic screening is nearly perfect on the surface of simple metals like Al, Mg and Na, the calculated face dependent surface energies are nearly independent of small displacement of the first lattice plane.(106)

Figure 15 shows the surface XANES of clean aluminum surfaces (111) and (100) compared with the bulk Al XANES of the $L_{2,3}$ edge.(17,107) The aluminum $L_{2,3}$ surface XANES spectra of the Al(100) and A(111) in the first 20 eV show differences due to the different surface partial density of states in the conduction band. These spectral changes are due both to the presence of an anisotropic potential at the surface and to the formation of surface states in the partial gaps in the surface projected bands. In particular the peaks at 77.1 eV and 84 eV in the Al(100) surface have been assigned(107) to surface resonances in the partial gaps of the projected bands at 4.3 eV and 10.5 eV above the Fermi energy. The maximum at about 97 eV in the spectra is due to the delayed threshold of the $2p \rightarrow \varepsilon d$ transitions and therefore its shift is partially due to the change of d bands at the surface. The minimum remains at the same energy (~104 eV) both in bulk aluminum and in Al(100) surface. This minimum at 32 eV above the Fermi energy was considered to be not sensitive to fine details of the electronic potential. Under this assumption and according with both the band structure and the multiple scattering approach discussed in section 2.1 and 2.2 the XANES peaks follow the expansion of the volume of the crystalline cell a^3, where a is the lattice parameter, following the rule

$$(E - V_0)\, a^2 = C \qquad (28)$$

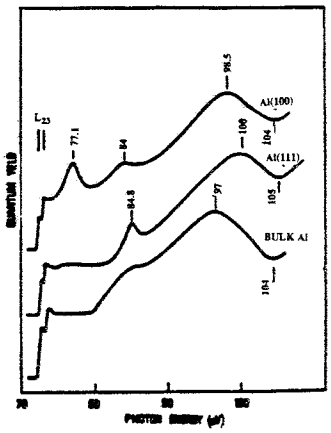

FIG. 15 - Surface soft x-ray absorption spectra of the Al(111) and Al(100) clean surfaces compared with the soft x-ray absorption spectrum of bulk aluminum.(107)

where E is the energy of peak in the absorption spectrum, V_o is the intersphere constant in the muffin tin approximation and C is a constant. As a consequence the spacings between the top layers for the Al(100) surface is the same as in the bulk. The fact that the Al(100) does not relax is confermed by several authors using Low Energy Electron Diffraction methods.(108,109)

The contraction versus the expansion of the Al(111) surface on the contrary is still object of discussion due to its small value. The shift of about 1 eV of the minimum in the Al(111) surface spectrum at 105 eV (see Figure 15) is an indication of a contraction of only 1.5% using the rule $\Delta E/(2(E-V_o)) = -\Delta R/R$, where the energy variation ΔE of the multiple scattering resonance is related with the small distance variation ΔR.(110) The LEED data shows no contraction, a slightly expansion (2.2%)(111) or a slight contraction.(109)

The different experimental results on aluminum surface can be affected by the different degree of "cleanness" of the surface and by the different surface sensitivity of the detection methods. Carring out surface XANES experiments the sensitivity is very high because by selecting a particular Auger energy close to the minimum of the escape depth, and the sampling depth is constant during the scan.

4.2 - XANES as a probe of atomic chemisorption on crystal surfaces

The determination of the structure of the chemisorption sites of different atomic species on the surface of oriented crystals is a key information for the surface science.

The surface absorption spectrum of an atom chemisorbed on the surface of a crystal can be measured by Auger electron yield, selecting the particular Auger line of the chemisorbed atomic species. The XANES spectra probe structural models of chemisorption sites via MS analysis or can provide a monitor of the structural changes at surfaces. XANES exhibits substantial advantages in comparison with other techniques because it can be measured for low adsorbate coverage (~1/100 monolayer).

Polarized Surface Extended X-ray Absorption Fine Structure (SEXAFS) provides direct information on bond distances between the chemisorption atom and the substrate. The joint analysis of the SEXAFS and XANES for solving chemisorption site structures is very important. In fact the bond distances obtained by SEXAFS should be used as input for XANES calculations which gives further information on the geometrical arrangements.

The first determination of a chemisorption site by surface XANES measurements interpreted by the multiple scattering theory has been the study of oxygen chemisorption on the single crystal Ni(100) surface.(65) This experiment shows that the surface XANES is a sensitive fingerprint of structural changes on the surface at different oxygen coverages. With increasing oxygen coverage on Ni(100) surface, different chemisorption geometries are produced, giving a p(2x2) or a c(2x2) LEED patterns. The XANES spectra make possible to

distinguish between different possible surface reconstructions.

The polarized oxygen K-edge XANES spectra of the chemisorbed oxygen on Ni(100) surface with increasing oxygen exposures are reported in Figure 16 for two different angles of incidence of the photon beam. The spectra exhibit a pronounced polarization dependence for low coverage which weakens for higher O exposures. At the highest oxygen coverage nickel oxide is formed. However the oxygen K-edge XANES spectrum of bulk NiO[74,112,113] is different from the spectrum of the saturated oxide layer formed by less than three layers.

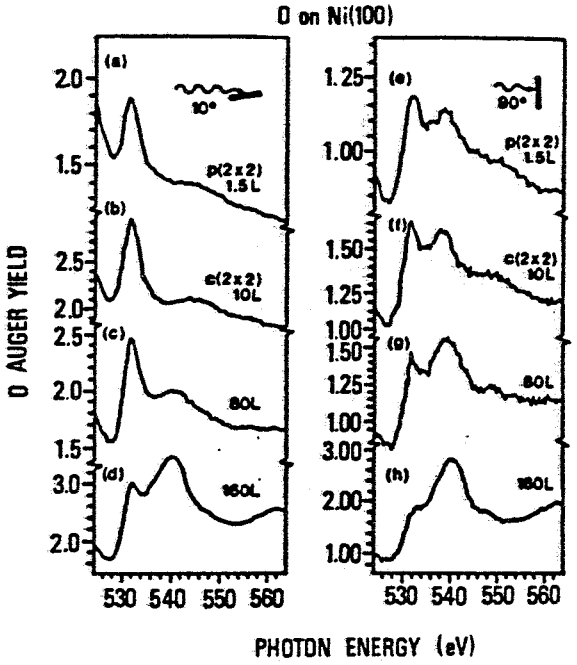

FIG. 16 - Oxygen K edge XANES spectra of oxygen chemisorbed on Ni(100) for increasing oxygen coverage (from 1.5L to 160L O_2) and two different x-ray grazing angles θ=10° (left panel) and θ=90° (rigth panel). For θ=10° the e vector makes an angle of 10° with the surface normal and it lies in the surface plane for θ=90°.[65]

The surface near edge spectra of O/Ni(100) were calculated using a computational scheme based on a cluster method in the frame of full multiple scattering.[44] The calculation was done for bulk Ni and for O atoms in a specific surface arrangements,[65] for a cluster including thirty neighboring atoms up to a distance >5.0 Å from the central O atom. Figure 17 shows the polarized experimental data for a c(2x2) O overlayer and the calculations assuming four different chemisorption sites. Calculations have been performed for atop, bridge and hollow sites (this last with $d_\perp$= 0.9 Å and $d_\perp$= 0.2 Å) with the bond length

constraint of 1.98 Å for the O-Ni distance as obtained by SEXAFS. It is possible to recognize from the figure that the calculated polarized spectra for hollow site with $d_{\perp} = 0.9$ Å is the one in better agreement with the experimental spectrum. This work has demonstrated that the XANES spectra of atomic adsorbates are not only dominated by nearest-neighbor atoms but larger clusters are necessary in the calculation.

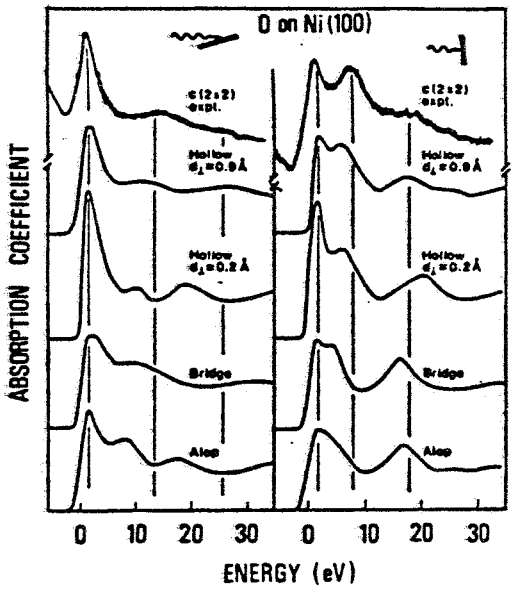

FIG. 17 - Comparison of the polarized experimental spectra (upper curves in the two panels, *expt.*) of c(2x2) oxygen chemisorbed on Ni(100) and the calculated XANES for four different chemisorption sites as indicated in the figure. (65)

The chemisorption of O on Cu(100) shows a 2x2 LEED pattern but different experimental measurements have yielded conflicting geometries for the c(2x2) reconstruction. This situation has been solved by quantitative XANES analysis in the framework of MS theory.(114,115) XANES spectra at the O K edge has shown that O in the c(2x2) overlayer occupies fourfold hollow sites with an O-Cu interlayer spacing of 0.7±0.1 Å, corresponding to an O-Cu bond length of ~1.9 Å.

The spectra of the O K edge for the Cu(100) c(2x2) are reported in Figure 18A and B for two different polar angles: $\theta=20°$ and $\theta=90°$, where θ is the angle between the electric field vector E and the surface normal. Both polarized spectra compared with full MS calculations(115) for the fourfold hollow, bridge and atop adsorption sites using the O-Cu bond length of 1.94(4)Å(116) and the truncated crystal structure for the substrate (a=3.615 Å) show that only fourfold hollow site is compatible with the experimental data. The

experimental profiles are well reproduced in both polarizations and in the θ=90° polarization the agreement of the peak positions is within 0.5 eV. The role of MS is shown comparing for each adsorption sites the results obtained by the corresponding curved-wave single scattering calculations (open circles in Figure 18). The spectra for θ=90° are insensitive to the O-Cu interlayer spacings while the spectra for θ=20° are sensitive to different $d_\perp$ values. In Figure 18C the experimental spectrum for θ=20° (upper curve) is compared with the calculated spectra for the fourfold hollow site for different values of $d_\perp$. The best agreement between experiment and theory gives $d_\perp = 0.7 \pm 0.1$ Å.

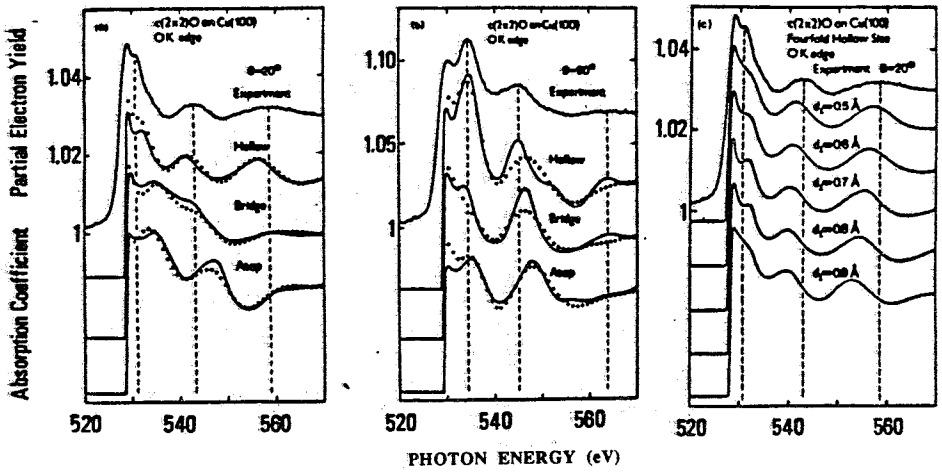

FIG. 18 - Comparison of measured (experiment) O K-edge XANES of c(2x2) O on Cu(100) for θ=20° (panel a) and θ=90° (panel b) with full multiple sacttering MS (solid lines) and single scattering (open circles) calculations for the fourfold hollow, bridge and atop adsorption sites.
Comparison of measured O K-edge XANES of c(2x2) O on Cu(100) for θ=20° with full MS calculations for several O-Cu interlayer spacings $d_{\perp}$ (panel c). (116)

The K-edge surface XANES of S chemisorbed on Ni(110) and on Ni(111) have been measured by Ohta et al.(117) by recording the S KLL Auger yield. A strong polarization dependence of the spectra has been found and the chemisorption site for the c(2x2) sulfur on Ni(110) has been determined. The analysis of the data for the reconstructed c(2x2) surface of S on Ni(110) shows that the sulfur atom is located on a hollow site.

4.3. - XANES of surface oxides

The investigation of the structure of the first disordered oxide layers formed on top of surfaces exposed to oxygen gas is of interest in understanding the microscopic process of

oxidation. The relevance of the structure determination of surface oxides for the technology of protective surface layers on metals and of the semiconductor-insulator or metal-insulator interfaces in electronics is well known.

The oxide layers formed on top of metals show in many cases a disordered structure that is not possible to investigate by diffraction methods because of the lack of long range crystaline order. On the contrary the XANES spectroscopy does not require crystalline order and it is site specific. Moreover the disordered structure makes more easy the interpretation of the experimental XANES data because it reduces the number of shells of neighbor atoms contributing to the spectrum. Therefore the XANES of amorphous surface oxide layers are determined mainly by the first shell. This last characteristic aspect of the XANES of amorphous oxides makes feasible the experimental determination of the symmetry of the coordination shell of the absorbing atom by using the empirical "finger print" approach. The measured spectrum of unkown compound is compared with the spectra of model compounds. The ideal model compounds should exhibit different coordination geometries of the absorbing atom and the number of neighbor shells contributing to their XANES spectra should be known.

The oxide formation on top of aluminum surface following the interaction of oxygen with the metal is a classical example of oxidation processes. The study of the transition from the chemisorption of the oxygen on clean Al surfaces to the oxidation phase upon oxygen exposure to aluminum single crystal was object of the first surface XANES experiment as shown in Figure 1.[17] The local structure of the first oxide layer formed on top of Al(100), Al(110) and Al(111) surfaces at oxygen exposures larger than 500 L has been determined by XANES.[4,17,118]

In Figure 19 the Al L_{23} surface x-ray absorption near edge spectra of Al-O complex on the Al(111) surface of the chemisorption phase at 100L oxygen exposure (upper panel) and of saturated oxide layer at 100L exposure at room temperature (solid line) measured by Auger quantum electron yield are shown. By XANES it possible to follow the change of the Al local structure from the chemisorption to the oxidation phase by increasing theoxygen coverage or by heat treatment starting from the chemisorption phase.

The dashed curves in Figure 19 show the surface XANES of the oxide-like cluster formed upon heating the sample to 400 °C. By XANES it easy to see that a surface oxide-like layer with similar Al-O coordination sites are obtained by heat treatment by starting both from the chemisorption phase as well as from the saturarted oxide phase.[118]

Information on the Al site structure in the oxide surface layer has been obtained by comparison of the Al $L_{2,3}$ XANES spectrum of the surface oxide with the spectra of amorphous a-Al_2O_3 where the Al ion has a fourfold tetrahedral coordination and with the spectrum of α–alumina where Al ion has an octahedral coordination shown in Figure 20. The spectrum of the surface oxide layer does not show a similarity with the spectrum of

amorphous alumina (a-Al_2O_3) ruling out the tetrahedral coordination for the Al ion. The analogies with the XANES of octahedrally coordinated Al in α–alumina indicate an octrahedral coordination for the first surface oxide layer. This result was not expected since the Al ion has a tetrahedral coordination in the thick amorphous surface oxide layers grown by electrolysis on aluminum. These conclusions have been confirmed by Norman et al.(119) by measuring the aluminum-oxygen distance of the surface oxide layer compared with a variety of aluminum oxide systems with tetrahedral and octahedral coordination using SEXAFS at the oxygen K edge.

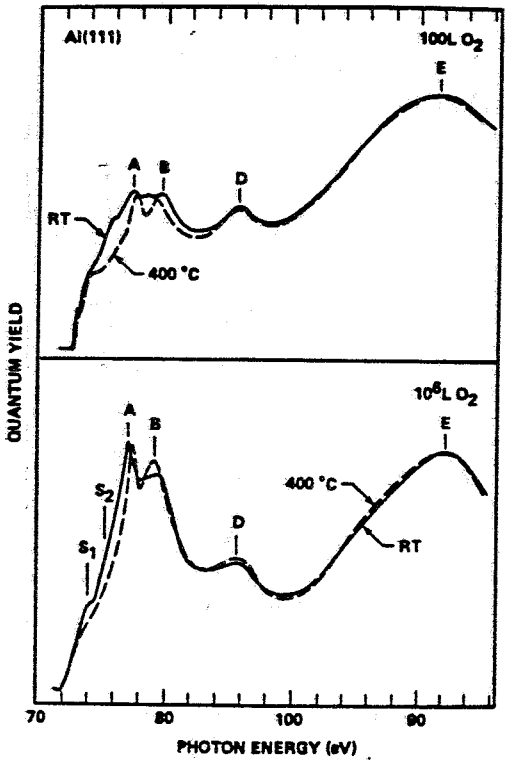

FIG. 19 - Al L_{23} surface x-ray absorption near edge spectra of Al-O complex on the Al(111) surface of the chemisorption phase at 100L oxygen exposure (upper panel) and of saturated oxide layer at 100L exposure at room temperature (solid line)measured by Auger quantum electron yield. The dashed curves show the surface XANES of the oxide-like cluster formed upon heating the sample to 400 °C. By XANES it easy to see that a surface oxide-like layer with similar Al-O coordination sites are obtained by heat treatment by starting both from the chemisorption phase as well as from the saturarted oxide phase.(118)

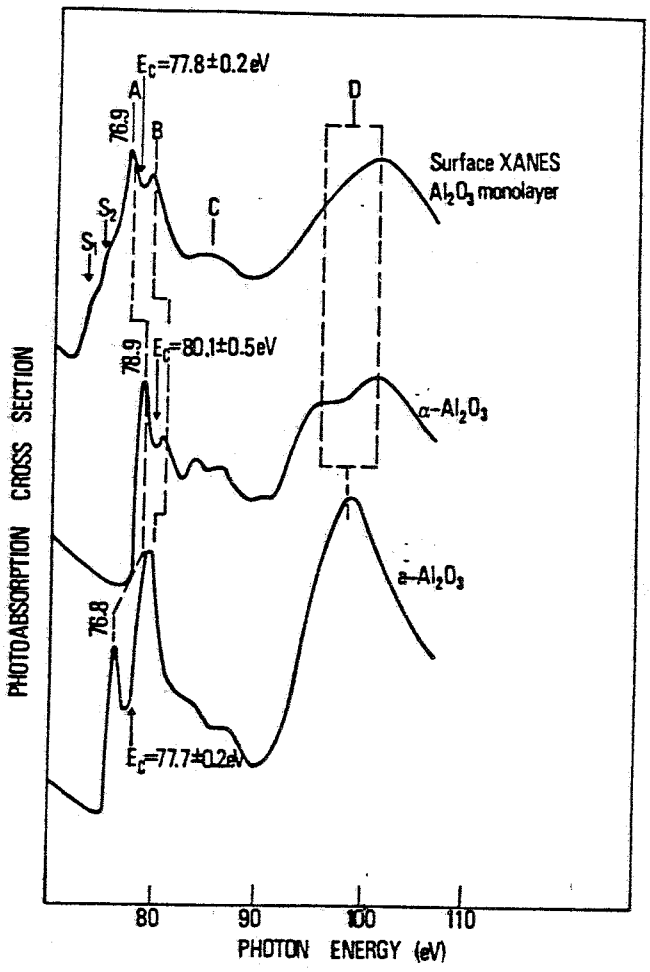

FIG. 20 - Surface XANES of the first oxide-like monolayer on Al(111), Al(100) and Al(110) surfaces (see FIG. 19) compared with the bulk x-ray absorption spectra of model compounds: amorphous a-Al_2O_3 and α-Al_2O_3 for determination of the local Al site structure by using the finger print approach. The energy E_c indicates the threshold for transition to continuum multiple scattering resonances.

A similar "finger print" approach was used to identify two different chemisorption sites for H^+ and F^+ ions on the α-Al_2O_3 polished parallel to the (0001) surface.(120) The XANES spectra measured by photon-stimulated desorption of H^+ and F^+ ions compared with the bulk spectrum measured by electron yield from α-Al_2O_3 substrate and amorphous alumina, are shown in Figure 21. The hydrogen and fluorine bonding sites clearly differ from each other and from the octahedral bulk α-Al_2O_3 site. The comparison with the bulk

spectra of model compounds shows that the hydrogen site is obviously tetrahedral, like in amorphous Al_2O_3, while the fluorine site has components similar to both tetrahedral and octahedral sites, suggesting a new site or a mixture of two.

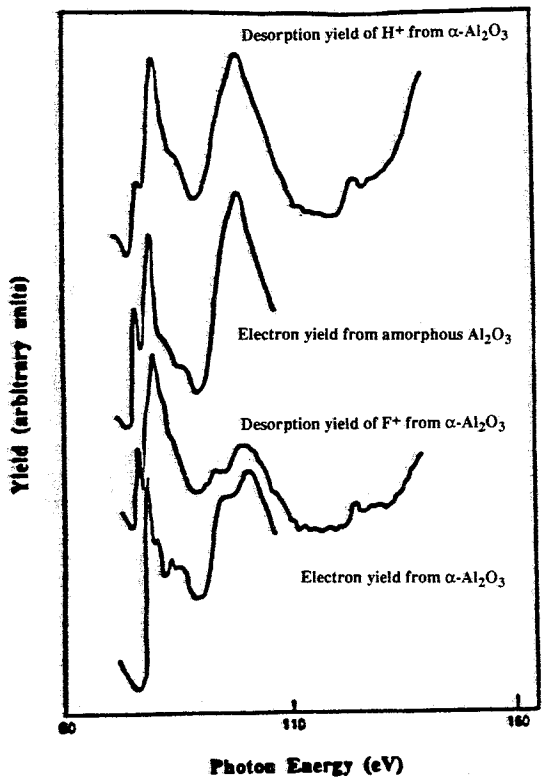

FIG. 21 - Photon stimulated desorption XANES aluminum L_{23} spectra. The desorption yield of H^+ and F^+ from α-Al_2O_3 and the electron yield from amorphous Al_2O_3 and α-Al_2O_3.

The silicon L_{23} edge spectrum of the first oxide on the Si(111) surface shows the formation of SiO_2-like oxide (formed by SiO_4 units) when the surface is exposed to oxygen at room temperature and the formation of a SiO-like surface oxide on the same silicon surface when the surface temperature rises above 700°C.[18] Figure 22 shows the L_3 spectra of surface silicon oxides. The spectrum of the oxide grown at room temperature is very similar to the bulk spectrum of silicon dioxide except for the peak named I which is due to transition at the silicon Si-SiO_2 interface. The spectrum of the surface oxide formed at high temperature shows large variation assigned to the formation of a local coordination around silicon like in SiO_x ($x \sim 1$).Therefore it was possible to determine the different local structure

of the first amorphous silicon oxide layer grown on top of silicon crystal at room and at high temperature. Moreover surface XANES provided a direct experimental evidence for a specific silicon site structure in the SiO_x oxide.

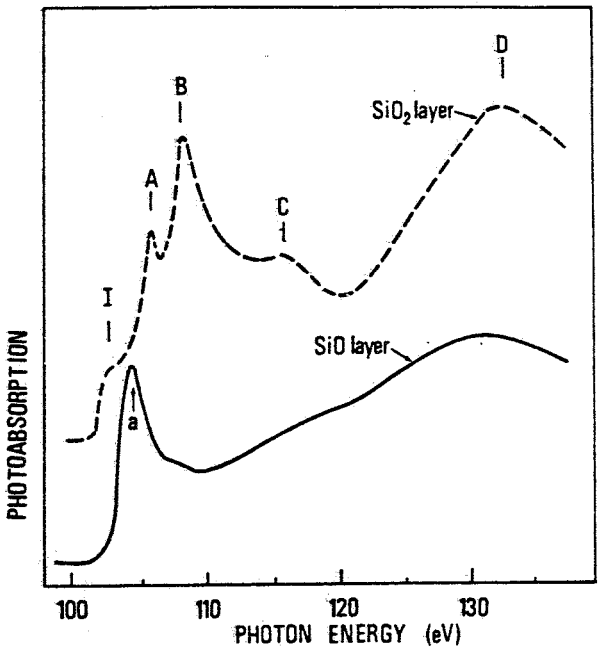

FIG. 22 - Comparison between the surface soft x-ray absorption of the saturated oxide layers formed on the Si(111) surface at room temperature ("SiO_2 layer" dashed curve) and of the oxide layer formed at 700°C ("SiO layer" full curve).

The local structure of the first nickel oxide layer formed on the nickel surface was studied by O K edge surface XANES.(113) Increasing oxygen exposure the O chemisorption phase is followed by the formation of the oxide phase for exposure larger than 150L as shown in Figure 16. The main difference between the spectrum of the surface oxide and that of the bulk NiO concerns mainly the quenching of the first peak A at the absorption threshold as shown in Figure 23. The intensity of this peak is a measure of the covalency of the nickel oxygen bond. In fact the ground state of NiO should be described by configuration interaction between $3d^8$ and $3d^9\underline{L}$ configurations (where $\underline{L}$ indicates a hole in the oxygen 2p orbital) because of the large electronic correlation. The first peak at the oxygen K threshold is due to the transition from the ground state to the final state configuration $O(\underline{1s})Ni(3d^9)$ (where the underline indicates the core hole).(74) Therefore its intensity is a measure of the

probability to find a hole in the oxygen 2p orbital i.e. of Ni-O covalency. The quenching of this peak was found also in defective $Ni_{(1-\delta)}O$ for δ=0.03, supporting the conclusion that the first surface oxide on Ni has a distorted structure in comparison with NiO crystal giving a less covalent nickel oxygen bond.

Using the total reflection method and the dispersive x-ray optics Dartyge et al.(92) performed in situ time resolved observation of surface modification of a copper "real" metal surface under chemical or elettrochemical treatments.

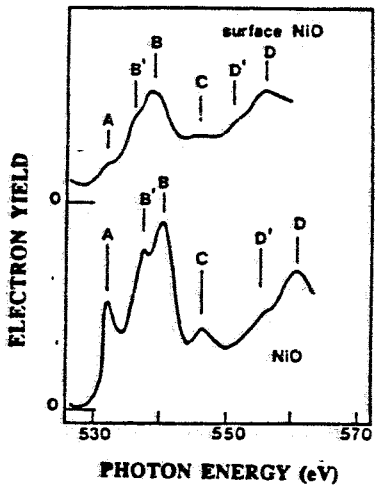

FIG. 23 - Oxygen K edge XANES of nickel oxide layer growth on Ni surface (top curve) compared with NiO (lower curve).

They followed the thermal oxidation of metal copper surface by annealing for two hours at 200°C a vapor deposited metallic film. The copper K edge XANES shows without ambiguity that this annealing treatment leads to Cu_2O oxide by comparison with model compound Cu_2O.

4.4. - XANES spectra of chemisorbed molecules

Core electron excitation spectra of gas-phase molecules have been studied for a long time by means of various experimental techniques. A complete list of available references in the field of gas-phase molecular core excitations can be found in reference 121.

In the molecular absorption spectra of low Z atoms a set of bound states are found below the ionization threshold. The most intense peaks fall within a Rydberg below the ionization threshold. These are bound states determined by transition to unfilled molecular orbitals, Rydberg states and multielectron shake-up final states. Above the ionization threshold other much broad resonances are observed. They were first assigned to "inner well resonances", due to an electronegative cage on the atoms surrounding the absorbing atom. Now they are better known as "shape resonances"(122,123) in fact they appear also at the K-edge of the covalent N_2 molecules. As discussed in section 2 these resonances are a particular case of multiple scattering resonances in the continuum which are determined by the geometrical

arrangement of the constituent atoms therefore can be used to study the structure of chemisorbed molecules on surfaces.

In Figure 24 the N K-edge spectrum of N_2 in a gas phase is shown.(39,124) Only one broad continuum shape resonance appears above the ionization threshold and a transition to a bound π state gives the sharpest peak at the threshold. Between these two transitions a set of excitations to bound states and double electron transitions (shake up transitions) in which, concomitant to the one-electron ionization process, another electron is promoted from an occupied valence orbital to an empty molecular orbital of the same symmetry type are observed. We focus our discussion on the shape resonance in the continuum.

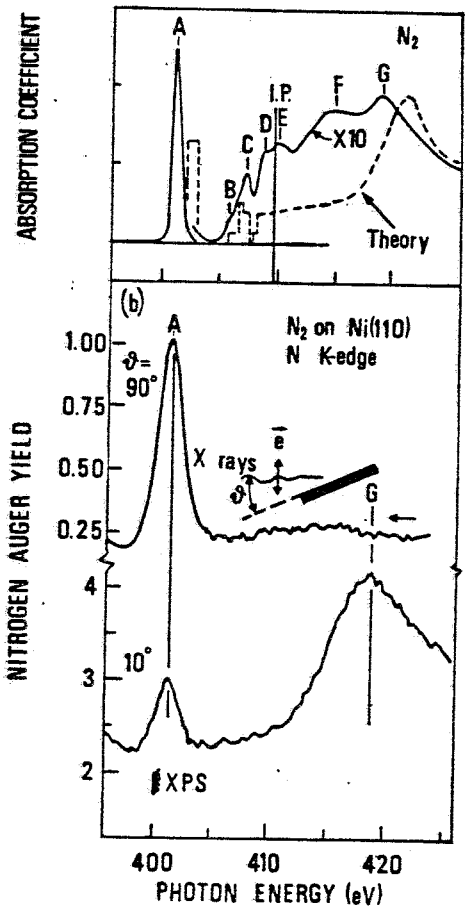

FIG. 24 - The upper panel shows the nitrogen K-edge absorption of N_2 gas compared with Dill and Dehmer MS calculation (dashed line).(39,124) The lower panel shows the polarized N K-edge of N_2 molecule chemisorbed on Ni(110) surface.(125)

The "shape resonance" for nitrogen molecule was first explained by Dehmer and Dill as a relative increase, around a particular energy, in the amplitude of the final state continuum wave function of σ symmetry near the photoionized atom in the molecule.(122,123) The final state electron is trapped in a quasi-bound state decaying away with a lifetime $\tau=h\Gamma_\gamma^{-1}$. Near edge structure arise from scattering processes within the "intramolecular" potential created by the atomic cores and the valence charge distribution of the molecule.

In the lower part of the Figure 24 the polarized spectra of N_2 chemisorbed at 90K on Ni(100) surface(125) for two different angles of incidence of the synchrotron radiation respect to the Ni surface are shown. The $\theta=10°$ degree spectrum of the chemisorbed molecule mainly show a σ-resonance while the $\theta=90°$ degree spectrum shows only the π-resonance.

The differences on the nitrogen spectra, induced by the chemisorption state, are the broadening of the σ-resonance and the disappearing of the all Rydberg and/or multielectron excitations. In general no new structures induced by the metal substrate are detectable.

Figure 24 shows the polarization dependence of the resonances and in particular the opposite behavior of the π and σ excitations caused by the vertical orientation of N_2 on the surface. The physical meaning of this dependence arise from the the fact that the σ-shape resonance involves final state which are symmetric respect to a reflection plane containing the molecular bond axis, on the contrary π-resonance involves antisymmetric final states respect to the same plane. Therefore in a photoabsorption spectra due to the dipole selection rules σ-shape resonance is maxima when the electric field **e** of the radiation is parallel to the bond axis while for polarization orthogonal to the bond the spectrum is featureless. Opposite to the σ-resonances, which are present in all molecules the π-resonances are due to transition of 1s electron into the antibonding π^* orbital. They are strongest if the **e** vector is parallel to the π orbital and give information on the hybridization of the bond. Accurate peak position analysis of the resonances should provide valuable information from the two final-state resonances in relation with change in the intramolecular bond length and distortions in molecular groups containing multiple bonds. Experimental evidence for the correlation between energy position of the σ resonances and bond lengths in the gas phase was found in hydrocarbons.(67,126)

The absorption spectra of molecules of the C_2H_n type with n=2, 4 and 6 are shown in Figure 25. The XANES of C_2H_2 and C_2H_4 were obtained by transmission measurements as a function of the gas pressure using synchrotron radiation.(126) The similar XANES spectra of C_2H_n have been measured by Hitchcock et al.(127) by electron energy loss spectroscopy.

The results of ab initio multiple scattering calculations for oriented N_2 and C_2H_n (n=2, 4, 6) molecules are reported in Figure 26, 27, 28 and 29. For each molecule, the z axis has been taken along the main bond (C-C or N-N) and in the case of the planar C_2H_4 the x axis was assumed to lie in the plane of the molecule. Polarized absorption cross sections (i.e. σ_x for **e//x**) and the total cross section (σ_{tot})for unpolarized spectra were calulated. The absorption cross section in the continuum above the ionization threshold are reported in the Figures 26-29.(128) The ionization threshold $E_t = (h\nu - I) = 0$ is determined with reference to a final state potential which is not self-consistently determined. The calculated energy position of the various continuum resonances from ionization threshold does not agree very well with experiments, despite this, the computed spectra clearly show the well known ℓ=3 resonance due to transition of a K shell electron to a continuum state of σ-symmetry when the polarization of the incident radiation is parallel to the axis of the molecule (z-polarization). In the calculations a resonance of ℓ=2 character due to the presence of the hydrogen atoms is present in both C_2H_4 and C_2H_6 spectra in transverse polarization (x polarization in C_2H_4 and x and y polarizations in C_2H_6). Despite their weak scattering power they are not entirely negligible. Recently identification of the C-H resonance in K-shell excitation spectra of free

ethylene and ethylene chemisorbed on various metal substrate at energies close to the ionization potential.(129)

In the frame of multiple scattering theory "shape resonances" in the cluster case are associated with singularities of the cluster K_C-matrix.(130) In the electron molecules scattering, as in the atomic case, resonances occur whenever some eigenvalue λ_m of the hermitian K_C-matrix goes to infinity. Under the assumption that the atomic phase shifts are smooth functions of E, which is always true in the energy region where atomic resonances are located, the approximate rule can be deduced for small variation of the interatomic distances R

$$k_r R = \text{constant} \tag{29}$$

where k_r is the resonance wavevector, R is the distance from the atomic scatterers in the cluster and the constant is determined by the details of the atomic scattering phase shift.

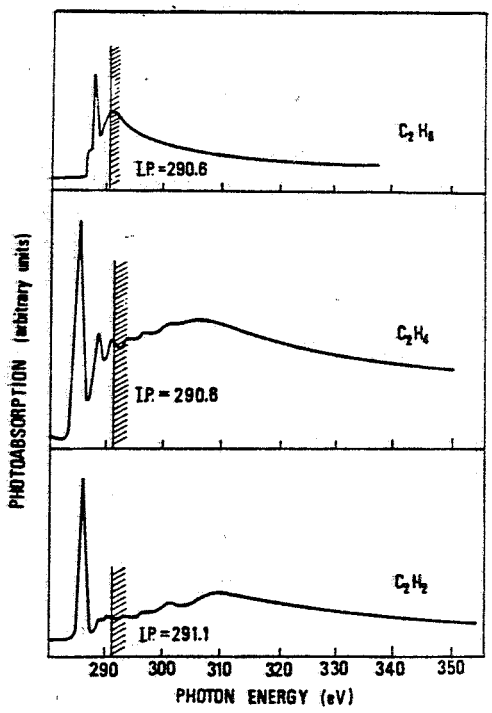

FIG. 25 - Experimental absorption spectra for C_2H_2, C_2H_4 and C_2H_6.(126) This latter spectrum is obtained by electron energy loss spectroscopy.

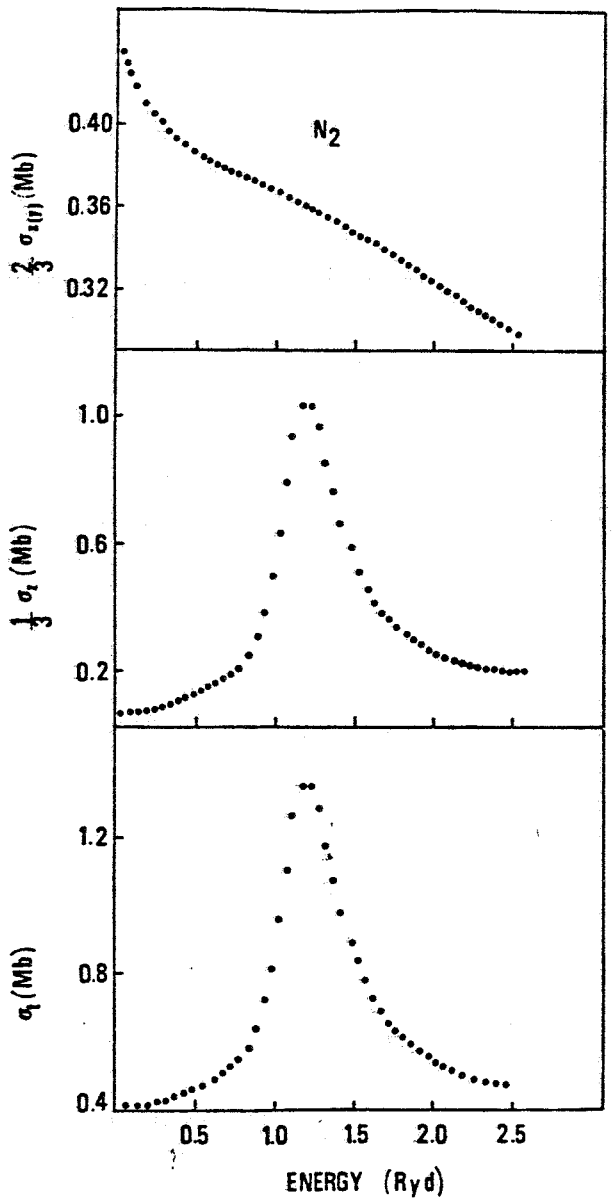

FIG. 26 - Calculated photoabsorption spectra for oriented N_2 molecule for longitudinal polarization $\sigma_z(E)$, transverse polarization $\sigma_x(E) = \sigma_y(E)$ and for random orientation $\sigma_{tot} = (\sigma_z+\sigma_x+\sigma_y)/3$.

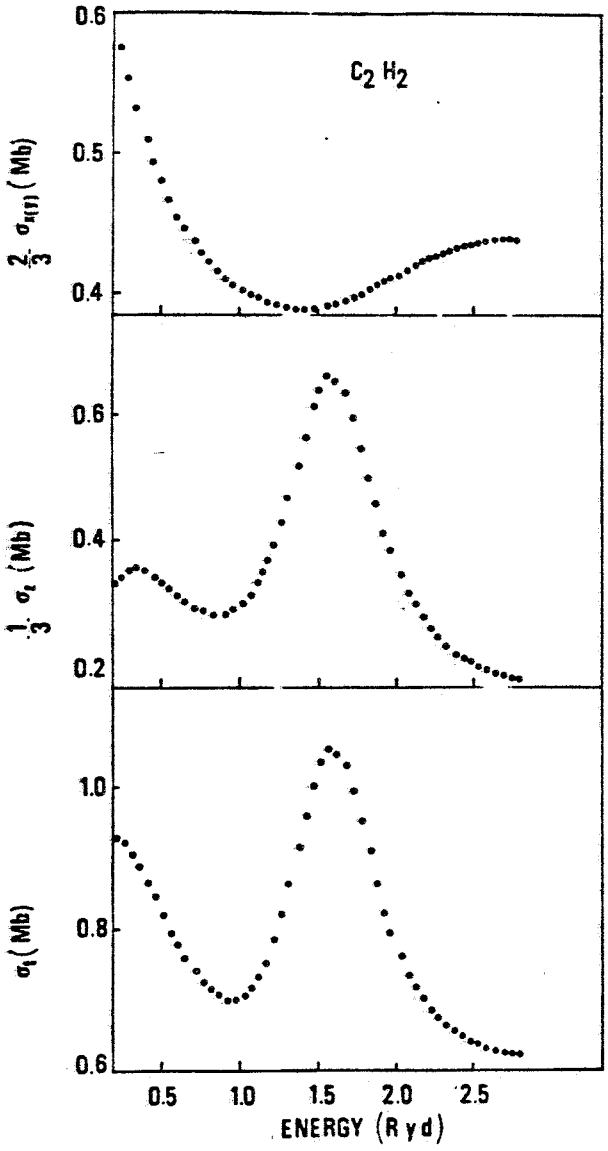

FIG. 27 - Same as FIG. 26 for C_2H_2 molecule.

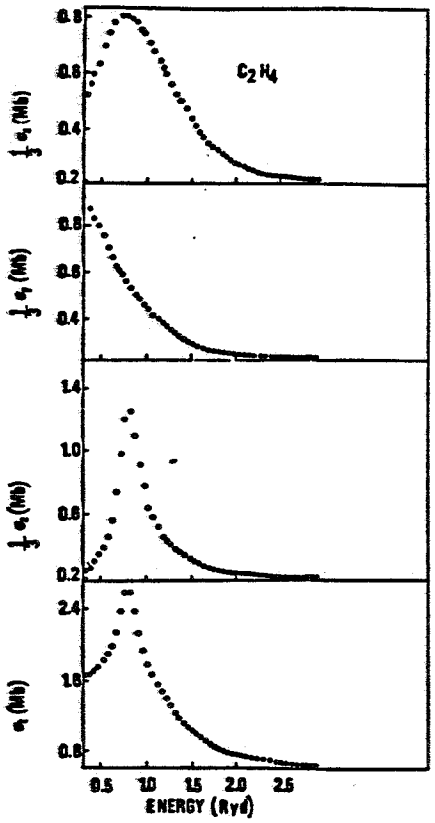

FIG. 28 - Same as FIG. 26 for C_2H_4 planar molecule. In this case $\sigma_z \neq \sigma_y$.

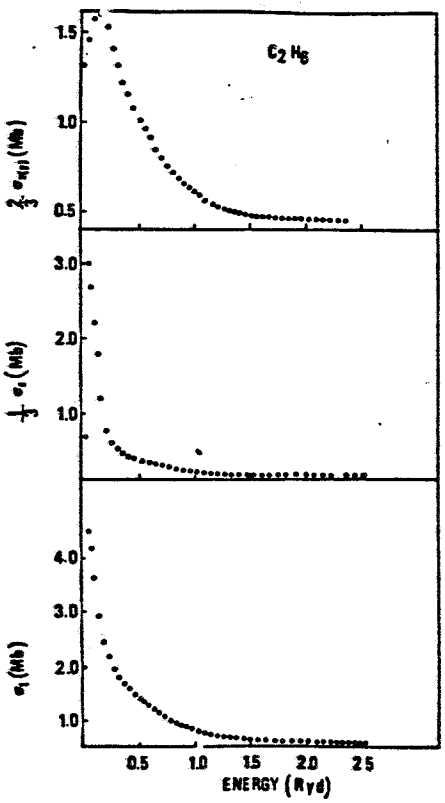

FIG. 29 - Same as FIG. 26 for C_2H_6 molecule.

This rule is verified in molecules or clusters with identical angular geometrical arrangement but different bond length scale, assuming that the phase shifts are "transferable" in the sense that they are functions only of the atomic species and rather insensitive to the environment. Very simple applications occur both in diatomic molecules (e.g. C_2H_n group neglecting hydrogen contributions) and in atomic clusters where the main MS resonance is due to the first coordination shell, at distance R from the photoabsorbing atom. The photoelectron wavevector k_r is referred to the average potential in the interstitial region between the ion cores V_0 (the "muffin tin zero") so that the simple relation (29) becomes

$$\int [E - V(r)]^{1/2} dr \sim [E - V_0]^{1/2} R = \text{constant} \qquad (30)$$

The near edge structure of the absorption spectra of molecular adsorbates are essential

dominated by intramolecular scattering with only small or negligible scattering contribution from the substrate atoms. A lot of chemical-physics processes are based on chemisorption process, for example the chemisorption on transition metals is the first step of many catalytic processes. Assuming that the interaction with the substrate is not strong enough to modify V_0 it is possible to determine the stretching of bond length in a molecule upon chemisorption. However caution must be used in order to extract bond distances from formula (30) because it is strictly valid only when the molecular geometry is the same and the variation of the interatomic distances are of the order of 10% or less. Different geometries give different MS resonances at different energies and large changes of interatomic distances induce changes in V_0 and in the phase shifts giving a different constant in the formula (30).

Figure 30 shows the absorption spectra at O K-edge for three molecules with carbon-oxygen bonds, chemisorbed on Cu(100).(66) The angle of the e vector to the surface has been chosen to maximize the intensity of the σ-shape resonance. The three molecular species are CO, with a short triple C-O bond (1.13 Å), formate (HCO_2), which is a pseudo-double C-O bond and metoxy (CH_3O), whith a longer single C-O bond (1.43 Å). At first approximation, hydrogen atoms may be ignored in this work. A π resonance peak is seen both for CO and formate close to O K-edge threshold, while no π character is detected in the single C-O bond for metoxy. The structure called X is not a weak π resonance but the atomic-like absorption step at the O K-edge. The energy position of the σ-shape resonance decreases with increasing C-O bond length. Using the rule (30) Stöhr et al. determined the unknown bond of the formate for the chemisorbed case.(66)

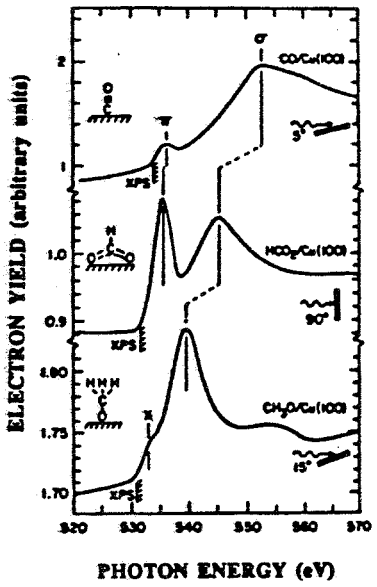

FIG. 30 - O K-edge XANES spectra of CO, HCO_2 and CH_3O on Cu(100). The angle of incidence is chosen in order to maximize the σ-shape resonance.(66)

Because the σ resonances arise from oxygen scattering with neighboring carbons, the scattering phase shifts were supposed identical in all three cases. Also the "muffin tin" constant V_0 was assumed to be the same in the molecule and in the chemisorption phase and independent on the bond distance. Using the value of bond change from triple C-O bond

between the σ-shape resonance excitation energy (E_σ) and the 1s binding energy (E_B) relative to the Fermi level E_f, was determined. The bond length extracted for the formate case was R=1.25±0.08 Å, to be compared with a simple linear approximation between σ-shape resonance excitation energy and R that yields to the value R=1.27±0.04 Å. This value is longer than in the gas phase, but in excellent agreement with the value R=1.25±0.02 Å for the C-O bond length in formate ions coordinated by a variety of metals, as a result of stronger interaction of the oxygen atoms with the substrate. This type of approach can give only a qualitative indication of the variation of bond distances. In fact in the XANES spectra of formate and metoxy cannot be compared because of the large geometrical difference.

Sette et al.(131,132) have empirically established for gas phase and for chemisorbed molecules containing low-Z atoms, that a linear relation between the energy of the shape resonance and bond length holds within several classes of molecules according to the number Z_t, defined as the sum of the atomic numbers of the absorber and the scatterers atoms (i.e. Z_t=12 for C-C bonds, while Z_t=14 includes molecules with N-N, B-F or C-O bonds).

A quantitative analysis of the carbon-carbon (C-C) distance variation from the gas phase to the chemisorption phase can be carried out in the case of chemisorption of hydrocarbons on metal surfaces. The rule (30) has been tested in the linear molecule C_2H_2 by performing several C K-shell multiple scattering calculations (with incident light polarized along the C-C bond) with different values of the C-C distance.(67)

In Figure 31 the experimental values of the energies of the σ resonances above the ionization potential for C_2H_2 and C_2H_4 in the gas phase and chemisorbed on Cu(100) at 60K(133) are reported versus $1/R^2$ where the interatomic C-C distance R has been measured also by SEXAFS in the same chemisorption phase.(134) A linear relation is found with V_o~22 eV. This value has been found by recent MS calculation for C-C distances in the range of 1.4÷1.5Å.(135)

A nice application of the near-edge spectroscopy for structural investigation is the study of the reaction intermediate states in the chemisortion process of hydrocarbons on Pt(111).(132) Figure 32A shows the near-edge structure at the C K-edge of condensed multilayers (90K) of two cyclic hydrocarbons: C_6D_{12} and C_7H_8, compared with the respective chemisorbed monolayer (170K) on Pt(111). For the cyclohexane system (C_6D_{12}) the multilayer and monolayer spectra are nearly identical, except for the Rydberg excitation at ~288 eV which is quenched by the interaction with the Pt(111) surface in the monolayer case. In these hydrocarbons both spectra are dominated by peak B, which is clearly assigned to the σ-shape resonance produced by the single C-C bond. For weakly chemisorbed molecules the σ resonance energy remains the same as in the gas phase to a very good approximation (≤ 1 eV) not only for simple diatomic molecules like N_2, CO and NO, on the contrary for the cycloheptatriene (C_7H_8) system, the multilayer spectra (90K) is characterized by a pronounced π resonance (A), two σ resonances B and C and the same Rydberg-type

excitation at ~288 eV that disappears in the monolayer spectra (230K). In this last case, while both σ resonances are almost unchanged at 230K, the peak A is strongly reduced in intensity. The presence in this ring shaped structure of single and double C-C bonds gives two σ-shape resonances, while the A peak is assigned to the transition to the corresponding π orbital. Using a linear rule between σ resonance positions and 1s binding energy the estimated R values are 1.51±0.03 Å for the C-C bond in C_6D_{12}, and 1.37±0.04 Å and 1.50±0.03 Å respectively for the double and single C-C bond in C_7H_8, very close to the respective gas-phase values and in agreement with prediction of higher stability for intramolecular bonding of ring structures.

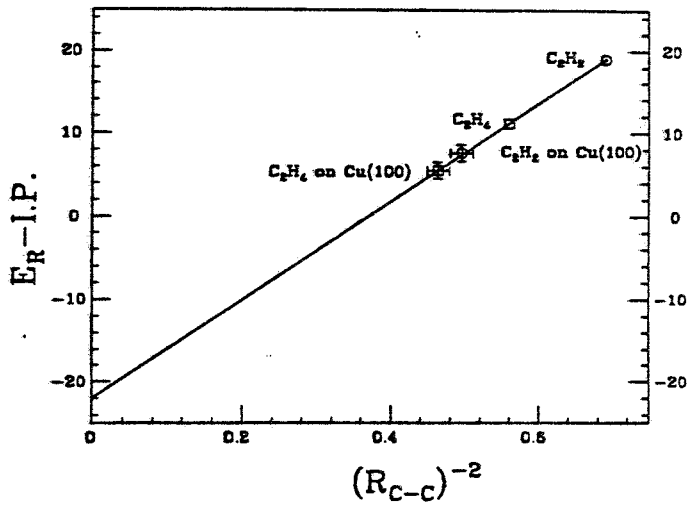

FIG. 31 - Linear relation between the σ resonance energy E_R and $(1/R)^2$, where R is the C-C distance for hydrocarbons C_2H_2 and C_2H_4 in the gas phase and in the chemisorbed phase on Cu(100).

In strong contrast with these values of ring-like structures are the R values extracted by the spectra reported in Figure 32B. The spectrum of ethylene (C_2H_4) on Pt(111) at monolayer coverage (90K) gives in fact a C-C bond length of 1.49±0.03 Å, with a stretching of 0.15 Å relative to the gas phase. Also for the acetylene (C_2D_2) the C-C distance is 1.49±0.03 Å, remarkably larger (0.25 Å) relative to the gas phase. These dramatic bond stretch show the presence in these molecules of a strong interaction of the π states with the metal surface.

XANES spectroscopy is a valuable local probe to study intramolecular bonding, molecular structure, orientation and hybridization of chemisorbed systems, however caution should be exercised in extending results to systems containing three or more collinear atoms such as CO_2, N_2O, NO_2 or COS, where multiple scattering effects play an important role and

where the molecular orbitals are partially spread out over all three atoms destroying the concept of resonant enhancement along a particular interatomic axis.

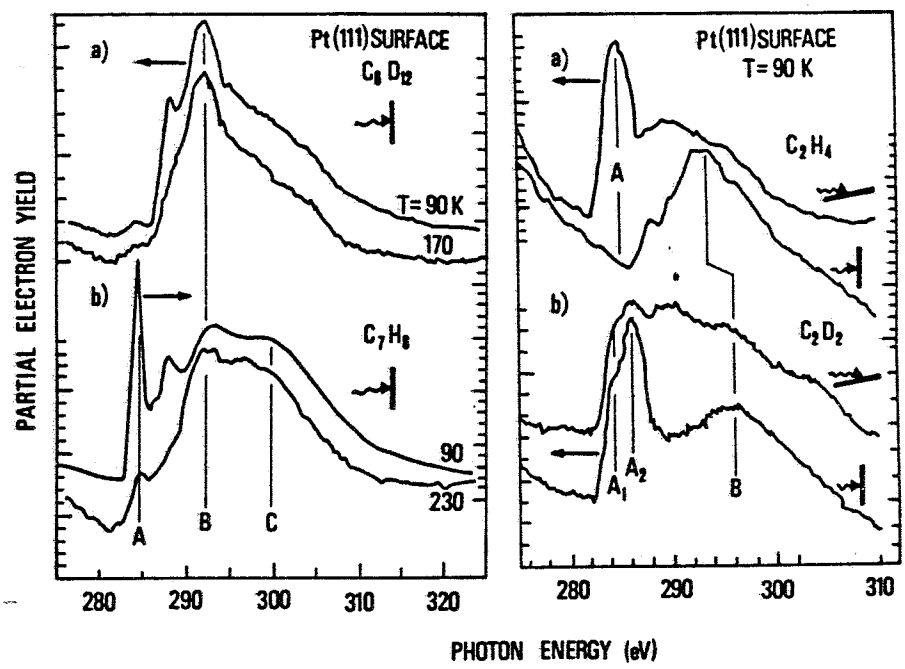

FIG. 32 - Left panel: a) Surface x-ray absorption spectra of cycloexane (C_6D_{12}) multilayer (T=90K) and monolayer (T=170K) on Pt(111) recorded at normal x-ray incidence; b) Spectra of cycloheptatriene (C_7H_8) as a multilayer (90K) and monolayer (230K) on Pt(111) for normal x-ray incidence.[132]
Right panel: a) Surface x-ray absorption spectra of ethylene (C_2H_4) on Pt(111) at saturation coverage at T=90K for grazing and normal x-ray incidence; b) Spectra of deuterated acetylene (C_2D_2) on Pt(111) under same condition as a).

4.5. - Molecular orientation on surfaces

Molecular chemisorption exhibits strong dependence of the resonance condition on the polarization of the incident radiation as already shown in the case on nitrogen and chemisorbed hydrocarbons. In the frame of multiple scattering theory the scattering matrix[130] is block diagonal and the off-diagonal elements between basis functions belonging to different irreducible representations are zero. Different polarization of incident light selects, through the Wigner-Eckart theorem the exact diagonal sub-block of the matrix

involved in the expression for the cross section. Polarization who select these particular sub-blocks present a resonance structure in the spectrum, which may be completely absent for other polarizations. This has been experimentally demonstrated in the photoabsorption spectra with polarized light for oriented molecules with cylindrical symmetry where for incident polarization along the bond, the absorption spectra presents a strong resonance feature (the well known ℓ=3 resonance), whereas for polarization orthogonal to the bond the spectrum is featureless.(125,136-138)

The problem of molecular orientation on surfaces has been widely studied by many experimental techniques. For example the orientation of chemisorbed carbon monoxide on metals like Ni surface is certainly one of the most popular topic in the surface science.

Figure 33A shows the absorption spectra near the C K-edge for a saturation coverage of CO on Ni(100), measured at different angles of incidence.(136) At normal incidence θ=90°, with the **e** vector parallel to the sample surface the resonance at 287.5 eV dominates the spectrum. Decreasing θ, the **e** vector rotates towards the surface normal, but while the peak A decreases a new resonance at 303.5 eV emerges and it is maxima at grazing incidence (θ=10°) where on the contrary peak A is almost vanished. Also the O K-edge spectra on the same system, reported in the Figure 33B, shows the similar behavior with the peak labeled A at 534 eV and the peak B at 550 eV. In both cases peaks B are readily assigned to the σ-shape resonance, because the molecular σ orbital is oriented along the molecular axis. The opposite polarization dependence identifies peak A as originating from transition from 1s state to the unfilled π^* bound molecular orbital state. As a consequence this transition is not detectable by photoemission experiment because lies below the continuum K-shell ionization threshold.

The intensity of these transitions can be derived from Fermi's golden rule which links the resonance intensity I to the matrix element of the photoabsorption cross section as given in formula (1) and (2). Therefore the cross section changes with the polarization angle θ as a function of the molecular orientation. Due to the dipole selections rule, and in the hypothesis of fully linearly polarized incident light we can write for an oriented molecule with cylindrical symmetry this simple cross section:

$$\mu(\delta) = \mu_o/4\pi \, [\, 1+1/2 \, \beta_m \, (3\cos^2 \delta - 1)] \qquad (31)$$

where μ_o is the integrated photoabsorption cross section for random molecular orientation and $\beta_m(h\nu)$ is an asymmetric parameter of molecular physics. Considering that δ is the angle between the **e** vector and the intramolecular symmetry axis, due to the form of β_m the photoabsorption cross section contains no interference term between σ and π ionization amplitudes, so that β_m=2 for s initial and σ final states, while β_m=-1 for s to π transitions giving respectively the simple relations $\mu \sim \cos^2 \delta$ and $\mu \sim \text{sen}^2 \delta$. Thus for a molecule oriented

along the surface normal the $\sigma(\pi)$ resonance should have a maximum for $\theta=0°(90°)$. Looking at Figure 33A the CO molecule stand upright on the Ni(100) surface. Possible deviations from the perfect angular dependence given above are due to a tilted molecular axis or to non linear component of the synchrotron radiation. In fact due to a small residual elliptical component of the polarization of the synchrotron radiation, the intensity of the peak A does not vanish completely for $\theta=0°$, but remains finite below $\theta\sim10°$ like shown in Figure 33 A and B.(137) A detailed analysis of the intensities of the σ and π resonances of the CO data as a function of polarization angles indicates a maximum deviation of the molecular axis from the sample normal of 10°, which is of the same order as the vibrational amplitude.(136) Results for CO provide the basis for the determination of the orientation of NO on Ni(100). X-ray absorption measurements for a saturation coverage of NO reported give identical results if compared with carbon monoxide experiment. Only one Ni atom, the one directly bonded to the C atoms seems to contribute to XANES spectra in molecular systems while the substrate contributions are negligibile, in great contrast with atomic adsorption, like in the case of oxygen where almost thirty neighbor atoms contributing to the spectrum.(65) Analysis of the intramolecular scattering in the molecular case gives quantitative information on the molecular bond lengths and the molecular orientation and it may be used to distinguish between molecular and atomic (dissociative) chemisorption.

The early stages of molecular dissociation are extremely important in the understanding of reaction chemistry. Oxidation has been studied on many metal surfaces, but controversial results has been obtained from different experimental techniques. The surface XANES are an ideal probe to investigate the molecular chemisorption and the detailed bonding and structure of the molecule. Stöhr et al. in the case of the controversial problem of the orientation of O_2 chemisorbed on Ag(110) and Pt(111) extracted the bond length of the molecular oxygen.(138) Figure 34A illustrates the spectra of oxygen in the case of chemisorption on Ag(110) at 90K, obtained by surface oxygen K-edge absorption spectra at various polar and azimuthal orientations of the electric field. All the spectra are characterized by a peak at 532.6 eV assigned to a transition from the O 1s core level to the unfilled σ^* antibonding orbital of the O-O bond. The lack of π^* resonance in the spectra indicates a complete filling of this orbital and shows the presence of single order O-O bond. The second weak peak observed around 542 eV in the spectra with the electric field along the [001] azimuth and with $\theta=90°$ is assigned to a scattering resonance due to the adsorbate-substrate bond. The analysis of the spectra reveals that the O_2 molecule lies approximately parallel to the surface with an uncertainty of 12° and parallel to the $[1\bar{1}0]$ azimuth. In fact the O-O σ^* peak is maximized when the electric field is parallel to the surface ($\theta=90°$) and to the $[1\bar{1}0]$ azimuth, giving directly the rough orientation of the bond. Also in this case more accurate analysis requires an exact knowledge of the polarization factor of the synchrotron radiation.(125,137) Figure 34B is referred to the O_2 on Pt(111) at 100K. Here the oxygen K-edge spectrum exhibits two

resonances: a σ^* resonance at 538.0 eV shifted by 5.4 eV if referred to the Ag(110) surface and a new π^* resonance at 531.1 eV. The correlation established between the position of the σ^* resonance and the intramolecular bond length in free and chemisorbed molecules gives an O-O bond length of 1.32±0.05 Å on Pt(111) and 1.47±0.05 Å on Ag(110), with a difference of 0.15±0.03 Å corresponding exactly to the 5.4 eV shift of the σ^* peak. These results shown that the O-O is a stretched bond oriented parallel to the surface, moreover the presence of a π^* peak for O_2 on Pt(111) is an indication of partly unfilled π^* orbital with a bond order larger than one. XANES analysis is in agreement with previous conclusion of vibrational and photoemission experiments, but in addition an accurate analysis of the bond lengths and of the intensities of the σ^* resonances should give a direct measure of the degree of rehybridization in these systems.

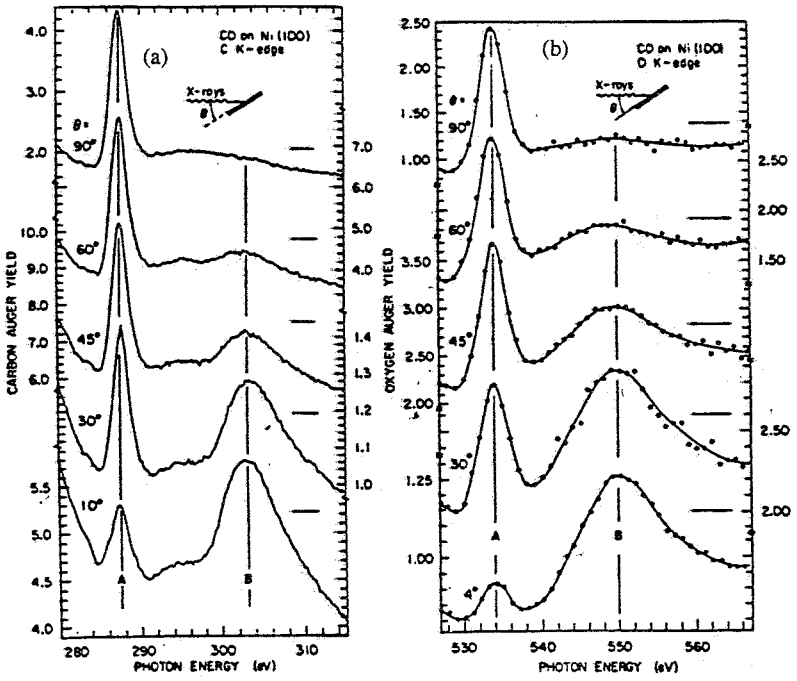

FIG. 33 - (A) Surface absorption spectra above the C K edge for CO on Ni(100) at T=180K as a function of grazing angle θ. (B) Surface absorption spectra above the O K edge for the same system as a function of incidence angle θ.

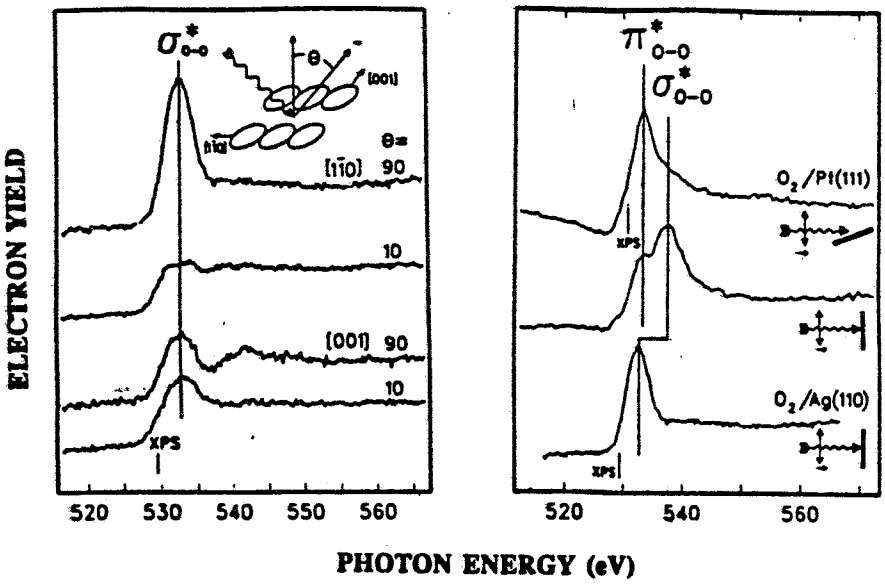

FIG. 34 - (A) Oxygen K-edge XANES spectra for O_2 on Ag(110) at 90K as a function of polar and azimuthal e orientations. The O-O σ^* peak at 532.6 eV is strongest when E lies along the O-O bond direction which occurs when e is along the [1 $\bar{1}$ 0] azimuth and parallel to the surface (θ=90°). The line at 529.3 eV marks the O(1s) binding energy relative to the Fermi level for O_2 on Ag(110).(138)
(B) XANES spectra for O_2 on Pt(111) at 100K(66) as a function of polar e orientation and in comparison to O_2 on Ag(110). The two peaks in the O_2/Pt(111) spectra are assigned to the O-O π^* resonance at 533.1 eV and to the O-O σ^* resonance at 538.0 eV and their angular dependence show that the O-O bond is parallel to the surface. Comparison with O_2/Ag(110) reveals a shift of the σ^* resonance, indicating a shorter O-O bond for O_2 on Pt(111). The line at 530.8 eV marks the O(1s) binding energy of O_2 on Pt(111).

XANES has been applied also to study complex molecular adsorbates to the determination of the structural transformation of the thiophene (C_4H_4S) molecule on the Pt(111) and Ni(100) surface as a function of the temperature, in order to study the dynamic of the hydrodesulfurization process.(96,139) Polarization dependent spectra at the C K edge in the framework of the dipole selection rules have shown that the thiophene molecule on Pt(111) at 150K is oriented with the ring plane tilted by about 40° from the surface, while after annealing process at 180K the molecule lies down to the surface. Careful analysis of the structure and of their broadening point out also a bonding to the metal through the π^* orbitals of the ring and an interaction of the Pt surface with the σ^* orbitals near the S atom in the case of parallel bonded molecules. The thermal decomposition process of the thiophene molecule on Pt(111) surface has been investigated in detail by comparison of the S L-XANES and the

L_{23} spectra at 180K corresponding to a monolayer coverage shows two well resolved structures X and Y respectively at about 166 and 174 eV. Increasing the anneal temperature peak X decreases in intensity and is almost undetectable at ~470K while peak Y has opposite behavior. The peak X is a resonance corresponding to transitions of S 2p electrons into unfilled π^* and σ^* molecular orbitals associated with the S-C bond in thiophene. Peak Y is an atomic S resonance in the continuum assigned to excitations to d-like final states.

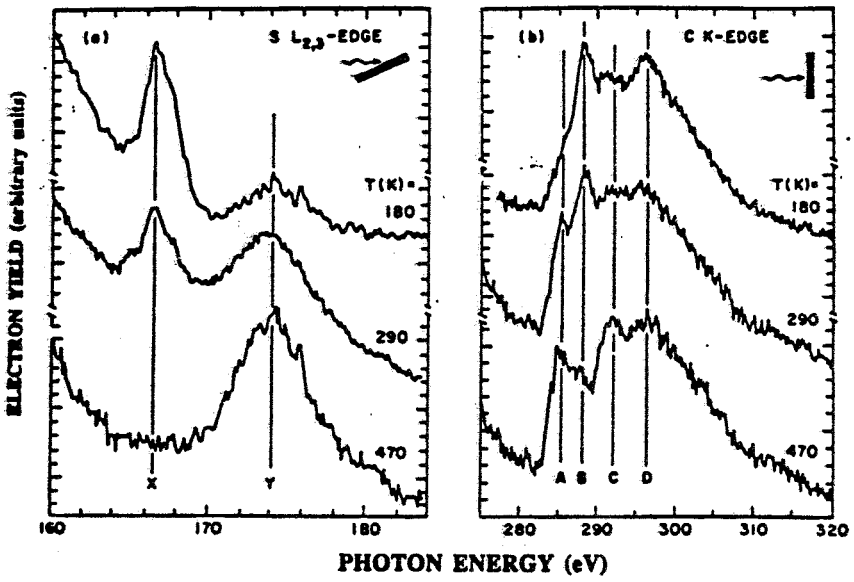

FIG. 35 - (Left panel b) XANES spectra at grazing x-ray incidence of the S $L_{2,3}$ edge for C_4H_4S on Pt(111) after annealing to different temperatures. Peak X represents a resonance characteristic of the C-S bond.(139)
(Right panel b) Spectra recorded for the C K edge under the same conditions as in (a). In this case the resonance associated with the C-S bond (peak B) disappears.

This behavior illustrated in Figure 35A indicates that thermal breaking of the C-S bond in the C_4H_4S molecule starts before 290K and it is completed at 470K. The C K-edge spectrum reported in Figure 35B strongly supports this conclusion, in addition peak B, assigned to a C-S bond follows the same trend of peak X in the sulfur spectra. Increasing temperature, evident cleavage of the C-S bond is accompanied by a reduction of peak D associated with C-C bonds and to the appearance of peak A. The peak A is shifted by 0.5 eV to lower energy from the π resonance of thiophene at lower temperatures as the result of the formation of molecular species, with a similar skeleton, but slightly inclined (<20°) relative to the surface

Additional information on the C-S bond breaking mechanism has been gained from the x-ray absorption study of thiophene adsorption on Ni(100).[96] XANES experiment performed by fluorescence photon yield, monitoring the S K_α made possible the detection of only one monolayer of thiophene, which corresponds to a sulfur sensitivity of about 0.08 monolayers. The study of dissociation of C_4H_4S on Ni(100) suggests a site-dependent C-S bond breaking on the clean Ni(100) surface with the thiophene ring dissociated after S interaction with the Ni surface. The presence of characteristic resonances shows that S atoms are bonded in the fourfold hollow Ni sites since a temperature of about 100K. The spectra at different coverages demonstrate that the first layer of dissociated molecules passivates the surface and at increasing coverage the molecules remains undissociated in the upper layers. The same mechanism is activated by the oxygen atoms so that when about half of the active fourfold hollow sites on the Ni surface are occupied (like in c(2x2) O reconstructed surface) no additional thiophene dissociation occurs.

These experiments show that polarization dependent x-ray absorption spectroscopy may probe not only the structure but also the nature of complex molecular reactions with metal surfaces like the hydrodesulphurization, which is one important industrial process. A new possibility for investigation of chemisorption processes occurring under real catalytic conditions.[96,97] is given by the fluorescence photon yield which allows the study of samples also in non-vacuum conditions up to high pressure and at extremely low coverage (<<0.1 monolayer). This technique have a sensitivity better than 1% of monolayer of CO with a detector designed to be used both in ultrahigh vacuum conditions or at gas pressure up to 10 Torr. The first x-ray absorption near edge structure measurements under atmospheric pressures was the investigation of the reactivity of CO with H_2 on Ni(100) detected by C K_α fluorescence photon yield.[95,96] Figure 36 shows typical results obtained at the C K-edge. The spectra (a) was taking in situ during an exposition of the Ni(100) surface to a mixture of $1x10^{-6}$ Torr CO and 0.1 Torr of H_2, while the spectra (b) is relative to a saturation under vacuum conditions with 10 L of H_2 followed by 20 L of CO. No significant change in the CO chemisorption geometry upon high pressure treatment are detected, like the ratio between glancing incidence spectra in the different conditions shows. Comparison of the data reasonably excludes any formation of intermediate species in the methanation reaction, no new surface compounds nor changes in bond angles or bond length are detected by XANES in this system. A careful analysis of the data indicates that exposure of carbon monoxide to high pressure of H_2 at room temperature results in the displacement of CO molecule from the surface, while if the Ni(100) is exposed to a CO-H_2 high pressure mixture CO molecules continue to chemisorb with their axis perpendicular to the surface as well known in UHV conditions.

The studies of chemisorption geometry of complex chemical organic conducting polymers like poly-3-methylthiophene electrochemically deposited on Pt surfaces by surface

XANES have carried out.(140) The polymeric chains were found to be well ordered on the metallic surface even for thickness up to 50Å. When the polymers are electrochemically doped to its conducting state the spectra show changes as function of thickness. These results in the field electrochemical interfaces show that this technique is now ready for a large number of different applications in surface science.

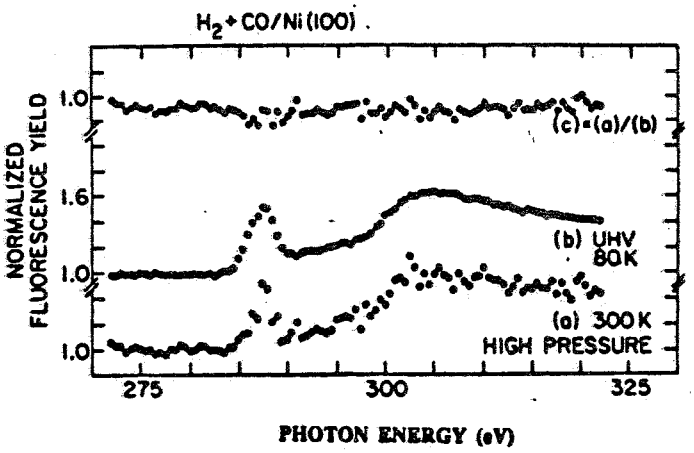

FIG. 36 - Normalized fluorescence yield XANES taken for coadsorbed hydrogen and CO on Ni(100) at room temperature under different pressure regimes: (a) continuous exposure to $1x10^{-6}$ Torr CO and 0.1 Torr H_2, (b) saturation under vacuum with 10 L H_2 first, followed by 20 L CO, (c) ratio between spectra (a) and (b).

REFERENCES

1. J. P. Pendry, Low Energy Electron Diffraction, Academic, New York (1974).
2. A. P. Lukirskii and I. A. Brytov, Investigation of the Energy Structure of Be and BeO by Ultra-Soft X-Ray Spectroscopy, Sov. Phys.-Solid State 6, 33-41 (1964).
3. W. Gudat and C. Kunz, Close similarity between Photoelectric Yield and Photoabsorption Spectra in the Soft-X-Ray range, Physic. Rev. Lett. 29, 169-172 (1972).
4. A. Bianconi, R. Z. Bachrach and S. A. Flodstrom, Study of the initial oxidation of single crystal aluminum by inter-atomic Auger yield spectroscopy, Solid State Commun. 24, 539-542 (1977).
5. P. A. Lee, Possibility of adsorbate position determination using final-state interference effects, Phys. Rev. B 13, 5261-5270 (1976).
6. U. Landman and D. L. Adams, Extended x-ray-absorption fine structure-Auger process for surface structure analysis: Theoretical considerations of a proposed experiment, Proc. Natl. Acad. Sci. USA 73, 2550-2553 (1976).
7. P. H. Citrin, P. Eisemberger and R. C. Hewitt, Extended X-Ray Absorption Fine Structure of Surface Atoms on Single-Crystal Substrates: Iodine Adsorbed on Ag(111), Phys. Rev. Lett. 41, 309-312 (1978).
8. J. Stöhr, D. Denley and P. Perfetti, Surface extended x-ray absorption fine structure in the soft-x-ray region: Study of an oxidized Al surface, Phys. Rev. B 18, 4132-4135 (1978).
9. A. Bianconi and R. Z. Bachrach, Al Surface Relaxation Using Surface Extended X-Ray Absorption Fine Structure, Phys. Rev. Lett. 42, 104-108 (1979).
10. R. Prinz and D. Konigsberger, X-ray Absorption: Principles and Techniques of EXAFS, SEXAFS and XANES, Wiley, New York (1986).
11. A. Bianconi, Surface X-ray Absorption Spectroscopy: Surface EXAFS and Surface XANES, Applications of Surface Science 6, 392-418 (1980).
12. J. Stöhr, EXAFS and Surface EXAFS: principles analysis and applications, in: Emission and Scattering Techniques, (P. Day, ed.), pp. 213-250, Reidel, Dordrecht (1981).
13. P. H. Citrin, An overview of SEXAFS during the past decade, in: EXAFS and Near Edge Structure IV, (P. Lagarde, D. Raoux and J. Petiau, eds.), J. Phys. (Paris) 47-C8, 437-472 (1986).
14. D. Norman, X-Ray absorption spectroscopy (EXAFS and XANES) at surfaces, J. Phys. C 19, 3273-3311 (1986).
15. J. Stöhr, SEXAFS: everything you always wanted to know about SEXAFS but were afraid to ask, in: X-ray Absorption: Principles and Techniques of EXAFS, SEXAFS and XANES, (R. Prinz and D. Konigsberger, eds.), pp. 443-571, Wiley, New York (1986).
16. J. Rowe, Surface EXAFS, in this volume
17. A. Bianconi, R. Z. Bachrach and S. A. Flodstrom, Oxygen chemisorption on Al: Unoccupied extrinsic surface resonances and site-structure determination by surface soft-x-ray absorption, Phys. Rev. B 19, 3879-3888 (1979).
18. A. Bianconi and R. S. Bauer, Evidence of SiO at the Si-oxide interface by surface soft x-ray absorption near edge spectroscopy, Surf. Science 99, 76-86 (1980).
19. U. von Barth and G. Grossmann, The effect of the core hole on x-ray emission spectra in simple metal, Solid State Commun. 32, 645-649 (1979).
20. U. von Barth and G. Grossmann, Dynamical effects in x-ray spectra and the final-state rule, Phys. Rev. B 25, 5150-5179 (1982).
21. A. Kotani, T. Jo and J. C. Parlebas, Many-body effects in core-level spectroscopy of rare-earth compounds, Adv. Phys. 37, 37-85 (1988).
22. U. Fano and J. W. Cooper, Spectral Distribution of Atomic Oscillator Strengths, Rev. Mod. Phys. 40, 441-507 (1968).
23. J. E. Müller, O. Jepsen and J. W. Wilkins, X-ray absorption spectra: K-edges of 3d transition metals, L-edges of 3d and 4d metals, and M-edges of palladium, Solid State Commun. 42, 365-368 (1982).

24. J. E. Müller and J. W. Wilkins, Band-structure approach to the x-ray spectra of metals, Phys. Rev. B 29, 4331-4348 (1984).
25. D. A. Papaconstantopoulos, Densities of States and Calculated K X-Ray Spectra of TiFe, Phys. Rev. Lett. 31, 1050-1052 (1973).
26. J. W. McCaffrey and D. A. Papaconstantopoulos, Calculated K X-Ray Absorption Spectrum of Calcium, Solid State Commun. 14, 1055-1058 (1974).
27. R. P. Gupta, A. J. Freeman and J. D. Dow, Band Theory of K-edge transitions in Li, Phys. Lett. 59A, 226-228 (1976).
28. R. P. Gupta and A. J. Freeman, Role of Band Structure on the X-Ray Edge-Shape in Na Metal, Phys. Lett. 59A, 223-225 (1976).
29. R. P. Gupta and A. J. Freeman, Band-Structure Contributions to X-Ray Emission and Absorption Spectra and Edges in Magnesium, Phys. Rev. Lett. 36, 1194-1197 (1976).
30. F. Szmulowicz and D. M. Pease, Augmented-plane-wave calculation and measurements of K and L x-ray spectra for solid Ni, Phys. Rev. B 17, 3341-3355 (1978).
31. J. E. Müller, O. Jepsen, O. K. Andersen and J. W. Wilkins, Systematic Structure in the K-Edge Photoabsorption Spectra of the 4d Transition Metals: Theory, Phys. Rev. Lett. 40, 720-722 (1978).
32. F. Szmulowicz and B. Segall, K x-ray absorption in aluminum, Phys. Rev. B 21, 5628-5635 (1980).
33. A. Bianconi, R. Del Sole, A. Selloni, P. Chiaradia, M. Fanfoni and I. Davoli, Partial density of unoccupied states and $L_{2,3}$-X-ray absorption spectrum of bulk silicon and of the Si(111) 2x1 surface, Solid State Commun. 64, 1313-1316 (1987).
34. G. A. Sawatzki, Electronic Structure of Transition Metal Compounds as Studied by High Energy Spectroscopies, in: Core Level Spectroscopy in Condensed Systems, (J. Kanamori and A. Kotani, eds.), pp. 99-124, Springer Verlag, Berlin (1988) and reference therein.
35. J. Fink, Th. Müller-Heinzerling, B. Scheerer, W. Speier, F. U. Hillebrecht, J. C. Fuggle, J. Zaanen and G. A. Sawatzki, 2p absorption spectra of the 3d elements, Phys. Rev. B 32, 4899-4904 (1985).
36. J. Zaanen, G. A. Sawatzki, J. Fink, W. Speier and J. C. Fuggle, $L_{2,3}$ absorption spectra of the lighter 3d transition metals, Phys. Rev. B 32, 4905-4913 (1985).
37. A. Bianconi, S. Doniach and D. Lublin, X-Ray Ca K-edge of calcium adenosine triphosphate system and of simple Ca compounds, Chem. Phys. Lett. 59, 121-124 (1978).
38. M. Belli, A. Scafati, A. Bianconi, S. Mobilio, S. Palladino, A. Reale and E. Burattini, X-Ray Absorption Near Edge Structures (XANES) in Simple and Complex Mn Compounds, Solid State Commun. 35, 355-361 (1980).
39. A. Bianconi, H. Petersen, F. C. Brown and R. Z. Bachrach, K-shell photoabsorption spectra of N_2 and N_2O using synchrotron radiation, Phys. Rev. A 17, 1907-1911 (1978).
40. D. Dill and J. L. Dehmer, Electron-molecule scattering and molecular photoioniztaion using the multiple-scattering method, J. Chem. Phys. 61, 692-699 (1974).
41. F. W. Kutzler, C. R. Natoli, D. K. Misemer, S. Doniach and K. O. Hodgson, Use of one-electron theory for the interpretation of near edge structure in K-shell x-ray absorption spectra of transition metal complexes, J. Chem. Phys. 73, 3274-3288 (1980).
42. C. R. Natoli, D. K. Misemer, S. Doniach and F. W. Kutzler, First-principles calculation of x-ray absorption-edge structure in molecular clusters, Phys. Rev. A 22, 1104-1108 (1980).
43. P. J. Durham, J. B. Pendry and C. H. Hodges, XANES: Determination of bond angles and multi-atom correlations in order and disorder systems, Solid State Commun. 38, 159-162 (1981).
44. P. J. Durham, J. B. Pendry and C. H. Hodges, Calculation of x-ray absorption near-edge structure, XANES, Comp. Phys. Commun. 25, 193-205 (1982).
45. R. V. Vedrinskii, L. A. Bugaev, I. I. Gegusin, V. L. Kraizman, A. A. Novakovich

R. E. Ruus, A. A. Maiste and M. A. Elango, X-Ray Absorption Near Edge Structure (XANES) for KCl, Solid State Commun. 44, 1401-1407 (1982).
46. T. Fujikawa, T. Matsuura and H. Kuroda,X-Ray Absorption Near Edge Structure (XANES) Studied by the Short-Range Order Multiple Scattering Theory, J. Phys. Soc. Jpn. 52, 905-912 (1983).
47. EXAFS and Near Edge Structure, (A. Bianconi, L. Incoccia and S. Stipcich, eds.) Springer Series in Chem. Phys. Vol. 27, Springer, Berlin (1983).
48. EXAFS and Near Edge Structure III, (K. O. Hodgson, B. Hedman and J. E. Penner-Hahn, eds.) Springer Proc. Phys. Vol. 2, Springer, Berlin (1984).
49. M. Kitamura, S. Muramatsu and C. Sugiura, Multiple-scattering approach to the x-ray absorption spectra of 3d transition metals, Phys. Rev. B 33, 5294-5300 (1986).
50. L. T. Wille, P. J. Durham and P. A. Sterne, X-ray absorption in ionic materials, in: EXAFS and Near Edge Structure IV, (P. Lagarde, D. Raoux and J. Petiau, eds.), J. Phys. (Paris) 47-C8, 43-47 (1986).
51. L. A. Bugaev, I. I. Gegusin, A. A. Novakovich and R. V. Vedrinskii, Crystal potential and size effects in XANES K-spectra of alkali halides, in: EXAFS and Near Edge Structure IV, (P. Lagarde, D. Raoux and J. Petiau, eds.), J. Phys. (Paris) 47-C8, 101-104 (1986).
52. R. F. Pettifer, D. L. Foulis and C. Hermes, Multiple scattering calculations for biological catalysts, in: EXAFS and Near Edge Structure IV, (P. Lagarde, D. Raoux and J. Petiau, eds.), J. Phys. (Paris) 47-C8, 545-550 (1986).
53. P. J. Durham, Theory of XANES, in: X-ray Absorption: Principles and Techniques of EXAFS, SEXAFS and XANES, (R. Prinz and D. Konigsberger, eds.), pp. 53-84, Wiley, New York (1986).
54. D. E. Sayers, E. A. Stern and F. W. Lytle, New Technique for Investigating Noncrystalline Structures: Fourier Analysis of the Extended X-Ray Absorption Fine Structure, Phys. Rev. Lett. 27, 1204-1207 (1971).
55. P. A. Lee and J. B. Pendry, Theory of the extended x-ray absorption fine structure, Phys. Rev. B 11, 2795-2811 (1975).
56. A. Bianconi, J. Garcia, A. Marcelli, M. Benfatto, C. R. Natoli and I. Davoli, Probing higher order correlation functions in liquids by XANES (X-Ray Absorption Near Edge Structure), J. Phys. 46-C9, 101-106 (1985).
57. J. Garcia, M. Benfatto, C. R. Natoli, A. Bianconi, I. Davoli and A. Marcelli, Three particle correlation function of metal ions in tetrahedral coordination determined by XANES, Solid State Commun. 58, 595-599 (1986).
58. M. Benfatto, C. R. Natoli, A. Bianconi, J. Garcia, A. Marcelli, M. Fanfoni and I. Davoli, Multiple-scattering regime and higher-order correlations in x-ray-absorption spectra of liquid solutions, Phys. Rev. B 34, 5774-5781 (1986).
59. A. Bianconi, A. Di Cicco, N. V. Pavel, M. Benfatto, A. Marcelli, C. R. Natoli, P. Pianetta and J. C. Woicik, Multiple-scattering effects in the K-edge x-ray absorption near-edge structure of crystalline and amorphous silicon, Phys. Rev. B 36, 6426-6433 (1987).
60. G. N. Greaves, P. J. Durham, G. Diakun and P. Quinn, Near-edge X-ray absorption spectra for metallic Cu and Mn, Nature 294, 139-142 (1981).
61. F. W. Kutzler, R. A. Scott, J. M. Berg, K. O. Hodgson, S. Doniach, S. P. Cramer and C. H. Chang, Single-Crystal Polarized X-Ray Absorption Spectroscopy. Observation and Theory for $(MoO_2S_2)^{2-}$, J. Am. Chem. Soc. 103, 6083-6088 (1981).
62. A. Bianconi, M. Dell'Ariccia, P. J. Durham and J. B. Pendry, Multiple-scattering resonances and structural effects in the x-ray-absorption near-edge spectra of FeII and FeIII hexacyanide complexes, Phys. Rev. B 26, 6502-6508 (1982).
63. J. E. Hahn, R. A. Scott, K. O. Hodgson, S. Doniach, S. R. Desjardins and E. I. Solomon, Observation of an electric quadrupole transition in the x-ray absorption spectrum of A Cu(II) complex, Chem. Phys. Lett. 88, 595-598 (1982).
64. R. A. Scott, J. E. Hahn, S. Doniach, H. C. Freeman and K. O. Hodgson, Polarized X-Ray Absorption Spectra of Oriented Plastocyanin Single Crystals. Investigation of

Methionine-Copper Coordination, J. Am. Chem. Soc. 104, 5364-5369 (1982).
65. D. Norman, J. Stöhr, R. Jaeger, P. J. Durham and J. B. Pendry, Determination of Local Atomic Arrangements at Surfaces from Near-Edge X-Ray-Absorption Fine Structure Studies: O on Ni(100), Phys. Rev. Lett. 51, 2052-2055 (1983).
66. J. Stöhr, J. L. Gland, W. Eberhardt, D. Outka, R. J. Madix, F. Sette, R. J. Koestner and U. Döbler, Bonding and Bond Lengths of Chemisorbed Molecules from Near-Edge X-Ray Absorption Fine-Structure Studies, Phys. Rev. Lett. 51, 2414-2417 (1983).
67. A. Bianconi, M. Dell'Ariccia, A. Gargano and C. R. Natoli, Bond Lenght Determination Using XANES, in: EXAFS and Near Edge Structure, (A. Bianconi, L. Incoccia and S. Stipcich, eds.), pp. 57-61, Springer Series in Chem. Phys. Vol. 27, Springer, Berlin (1983).
68. A. Bianconi, A. Congiu-Castellano, P. J. Durham, S. S. Hasnain and S. Phillips, The CO bond angle of carboxymyoglobin determined by angular-resolved XANES spectroscopy, Nature 318, 685-687 (1985).
69. D. D. Vvedensky and J. B. Pendry, Comment on "Experimental Study of Multiple Scattering in X-Ray-Absorption Near-Edge Structure", Phys. Rev. Lett. 54, 2725 (1985).
70. A. Bianconi, E. Fritsch, G. Calas and J. Petiau, X-ray-absorption near-edge structure of 3d transition elements in tetrahedral coordination: The effect of bond-length variation, Phys. Rev. B 32, 4292-4295 (1985).
71. D. Norman, K. B. Garg and P. J. Durham, The X-Ray Absorption Near Edge Structure of transition Metal Oxides: A One-Electron Interpretation, Solid State Commun. 56, 895-898 (1985).
72. H. Oizumi, J. Iizuka, H. Oyanagi, T. Fujikawa, T. Ohta and S. Usami, K-Edge XANES of GaP, InP and GaSb, Jpn. Journ. Appl. Phys. 24, 1475-1478 (1985).
73. T. A. Smith, J. E. Penner-Hahn, M. A. Berding, S. Doniach and K. O. Hodgson, Polarized X-ray absorption edge spectroscopy of single-crystal copper(II) complexes, J. Am. Chem. Soc. 107, 5945-5955 (1985).
74. I. Davoli, A. Marcelli, A. Bianconi, M. Tomellini and M. Fanfoni, Multielectron configurations in the x-ray absorption near-edge structure of NiO at the oxygen K threshold, Phys. Rev. B 33, 2979-2982 (1986).
75. M. Kitamura, C. Sugiura and S. Muramatsu, X-Ray-Absorption Near-Edge-Structure Study of Diamond: A Multiple-Scattering Approach, Solid State Comm. 62, 663-665 (1986).
76. S. Stizza, M. Benfatto, A. Bianconi, J. Garcia, G. Mancini and C. R. Natoli, in: EXAFS and Near Edge Structure IV, (P. Lagarde, D. Raoux and J. Petiau, eds.), J. Phys. (Paris) 47-C8, 691-696 (1986).
77. Biophysics and Synchrotron Radiation, (A. Bianconi and A. Congiu Castellano, eds.), Springer Series in Biophysics Vol. 2, Springer, Berlin (1987).
78. K. H. Johnson, Multiple-Scattering Model for Polyatomic Molecules, J. Chem. Phys. 45, 3085-3095 (1966); Scattered-Wave Theory of the Chemical Bond, Adv. Quantum Chem. 7, 143-185 (1973)
79. E. Clementi and C. Roetti, Roothan-Hartree-Fock Atomic Wavefunctions, in: Atomic Data and Nuclear Data Tables, pp. 177-478, Vol. 14, Academic, New York (1974).
80. K. Schwartz, Optimization on the Statistical Exchange Parameter α for the Free Atoms of H through Nb, Phys. Rev. B 5, 2466-2468 (1972).
81. L. Hedin and B. I. Lundqvist, Explicit local exchange-correlation potentials, J. Phys. C 4, 2064-2083 (1971).
82. C. R. Natoli, M. Benfatto and S. Doniach, Use of general potentials in multiple scattering theory, Phys. Rev. A 34, 4682-4694 (1986).
83. W. L. Schaich, Derivation of single-scattering formulas for x-ray-absorption and high-energy electron-loss spectroscopies, Phys. Rev. B 29, 6513-6519 (1984).
84. C. R. Natoli and M. Benfatto, A unifying scheme of interpretation of x-ray absorption spectra based on the multiple scattering theory, in: EXAFS and Near Edge Structure IV, (P. Lagarde, D. Raoux and J. Petiau, eds.), J. Phys. (Paris) 47-C8, 11-23 (1986).

85. M. Benfatto, C. R. Natoli, C. Brouder, R. F. Pettifer and M. F. Ruiz Lopez, Polarized curved wave EXAFS: Theory and application, Phys. Rev. B 39, 1936-1939 (1989)
86. J. J. Rehr, R. C. Albers, C. R. Natoli and E. A. Stern, New high-energy approximation for x-ray-absorption near-edge structure, Phys. Rev. B 34, 4350-4353 (1986).
87. J. J. Boland, S. E. Crane and J. D. Baldeschwieler, Theory of extended x-ray absorption fine structure: Single and multiple scattering formalisms, J. Chem. Phys. 77, 142-153 (1982).
88. B. K. Teo, Bond Angle Determination by EXAFS: A New Dimension, in: EXAFS and Near Edge Structure, (A. Bianconi, L. Incoccia and S. Stipcich, eds.), pp. 11-21, Springer Series in Chem. Phys. Vol. 27, Springer, Berlin (1983).
89. A. Di Cicco, N.V. Pavel and A. Bianconi, Spherical wave EXAFS analysis of the silicon K-edge x-ray absorption spectrum, Solid State Commun. 61, 635-639 (1987).
90. R. Barchewitz, M. Cremonese-Visicato and G. Onori, X-ray photoabsorption of solids by specular reflection, J. Phys. C 11, 4439-4445 (1978).
91. S. M. Heald, E. Keller and E. A. Stern, Fluorescence Detection of Surface EXAFS, Phys. Lett. 103A, 155-158 (1984).
92. E. Dartyge, A. Fontaine, G. Tourillon, R. Cortes and A. Jucha, X-Ray Absorption Spectroscopy in Dispersive Mode and By Total Reflection, Phys. Lett. 113A, 384-388 (1986).
93. J. Stöhr, C. Noguera and T. Kendelewicz, Auger and photoelectron contributions to the electron-yield surface extended x-ray-absorption fine-structure signal, Phys. Rev. B 30, 5571-5579 (1984).
94. V. Rehn and R. Rosenberg, Photo-desorption, this volume
95. F. Zaera, D. A. Fischer, S. Shen and J. L.Gland, Fluorescence Yield Near-Edge X-Ray Absorption Spectroscopy under Atmospheric Conditions: CO and H_2 Coadsorption on Ni(100) at Pressures between 10^{-9} and 0.1 Torr, Surf. Science 194, 205-216 (1988).
96. J. Stöhr, E. B. Kollin, D. A. Fischer, J. B. Hastings, F. Zaera and F. Sette, Surface Extended X-Ray Absorption Fine Structure of Low Z Adsorbates Studied with Fluorescence Detection, Phys. Rev. Lett. 55, 1468-1471 (1985).
97. D. A. Fischer and J. L. Gland, Soft X-Ray Fluorescence (UHV Compatible) Proportional Counters for NEXAFS and SEXAFS above the C, N, O and S K edge. in: Soft X-Ray Optics and Technology, SPIE 733, (1986), pp. 504-507.
98. D. A. Fischer, U. Döbler, D. Arvanitis, L. Wenzel, K. Baberschke and J. Stöhr, Carbon K-edge Structure of Chemisorbed Molecules by Means of Fluorescence Detection, Surface Science 177, 114-120 (1986).
99. D. Arvanitis, U. Döbler, L. Wenzel, K. Baberschke and J. Stöhr, A new tecnique for submonolayer NEXAFS: Fluorescence yield at the carbon K edge, in: EXAFS and Near Edge Structure IV, (P. Lagarde, D. Raoux and J. Petiau, eds.), J. Phys. (Paris) 47-C8, 173-178 (1986).
100. R. P. Phizackerley, Z. U. Rek, G. B. Stephenson, S. D. Conradson, K. O. Hodgson, T. Matsushita and H. Oyanagi, An energy-dispersive spectrometer for the rapid measurement of x-ray absorption spectra using synchrotron radiation, J. Appl. Crystallog. 16, 220-232 (1983).
101. K. C. Pandey, New π-bonded chain model for Si(111)-(2x1) surface, Phys. Rev. Lett. 47, 1913-1917 (1981).
102. K. C. Pandey, Reconstruction of semiconductor surfaces: buckling, ionicity, and π-bonded chains, Phys. Rev. Lett. 49, 223-226 (1982).
103. J. C. Woicik, B. B. Pate and P. Pianetta, Silicon(111) 2x1 Surface States: K-edge Transitions and Surface Selective $L_{2,3}$VV Auger Lineshape, Proceedings Vth International XAFS Conference, Seattle (1988).
104. M. Hietschold, G. Paash and I.Bartos, Adiabatic variational calculation of the lattice relaxation at metal surfaces, Phys. Status Solidi B 101, 239-252 (1980).
105. U. Landman, R. N. Hill and M.Mostoller, Lattice relaxation at metal surfaces: An

electrostatic model, Phys. Rev. B 21, 448-457 (1980).
106. J. P. Perdew, Physics of lattice relaxation at surfaces of simple metals, Phys. Rev. B 25, 6291-6299 (1982).
107. R. Z. Bachrach, D. J. Chadi and A. Bianconi, Unoccupied Surface Resonances on Aluminum Single Crystal Surfaces, Solid State Commun. 28, 931-934 (1978).
108. D. W. Jepsen, P. M. Marcus and F. Jona, Accurate calculation of the low-energy electron-diffraction spectra of Al by the Layer-Korringa-Kohn-Rostoker method, Phys. Rev. Lett. 26, 1365-1368 (1971).
109. P. E. Vilijoen, B. J. Wessels, G. L. P. Berning and J. P. Roux, Temperature dependent low energy electron diffraction from aluminum, J. Vac. Sci. Tech. 20, 204-212 (1982); and references therein.
110. A. Bianconi, XANES spectroscopy for Local Structures in Complex Systems, in: EXAFS and Near Edge Structure, (A. Bianconi, L. Incoccia and S. Stipcich, eds.), pp. 118-129, Springer Series in Chem. Phys. Vol. 27, Springer, Berlin (1983).
111. F. Jona, D. Sondericker and P. M. Marcus, Al(111) revisited, J. Phys. C 13, L155-L158 (1980).
112. L. A. Grunes, R. D. Leapman, C. N. Wilker, R Hoffmann and A. B. Kunz, Oxygen K near-edge fine structure: an electron-energy-loss investigation with comparison to new theory for selected 3d transition-metal oxides, Phys. Rev. B 25, 7157-7173 (1982).
113. I. Davoli, M. Tomellini and M. Fanfoni, Surface Ni oxide studied by oxygen K-XANES, in: EXAFS and Near Edge Structure IV, (P. Lagarde, D. Raoux and J. Petiau, eds.), J. Phys. (Paris) 47-C8, 517-520 (1986).
114. D. D. Vvedensky, D. K. Saldin and J. B. Pendry, Un update of DLXANES, the calculation of X-ray absorption near edge structure, Comput. Phys. Commun. 40, 421-424 (1986).
115. D. D. Vvedensky, J. B. Pendry, U. Döbler and K. Baberschke, Quantitative multiple scattering analysis of near-edge x-ray-absorption fine structure: c(2x2)O on Cu(100), Phys. Rev. B 35, 7756-7759 (1987).
116. U. Döbler, K. Baberschke, J. Stöhr and D. A. Outka, Structure of c(2x2) oxygen on Cu(100): A surface extended x-ray absorption fine-structure study, Phys. Rev. B 31, 2532-2534 (1985).
117 T. Ohta, Y. Kitajima, P. M. Stefan, M. L. Shek Stefan, N. Kosugi and H. Kuroda, Surface EXAFS and XANES Studies of S/Ni(110) and S/Ni(111), in: EXAFS and Near Edge Structure IV, (P. Lagarde, D. Raoux and J. Petiau, eds.), J. Phys. (Paris) 47-C8, 503-508 (1986).
118. A. Bianconi, R. Z. Bachrach, S. B. M. Hagstrom and S. A. Flodstrom, Al-Al_2O_3 interface study using surface x-ray absorption and photoemission spectroscopy, Phys. Rev. B 19, 2837-2843 (1979).
119. D. Norman, S. Brennan, R. Jaeger and J. Stöhr, Structure models for the interaction of oxygen with Al(111) and Al implied by photoemission and surface EXAFS, Surf. Science 105, L297-L306 (1981).
120. M. L. Knotek, R. H. Stulen, G. M. Loubriel, V. Rehn, R. A. Rosemberg and C. C. Parks, Photon stimulated desorption of H^+ and F^+ from BeO, Al_2O_3 and SiO_2: comparison of near edge structure to photoelectron yield, Surf. Science 133, 291-304 (1983).
121. A. P. Hitchcock, Bibliography of Atomic and Molecular Inner-shell Excitation Studies, an update of: J. Electron Spectrosc.& Relat. Phenom. 25, 245-275 (1982).
122. J. L. Dehmer and D. Dill, Shape resonances in K-Shell Photoionization of Diatomic Molecules, Phys. Rev. Lett. 35, 213-215 (1975).
123. J. L. Dehmer and D. Dill, Molecular effects on inner-shell photoabsorption. K-shell spectrum of N_2, J. Chem. Phys. 65, 5327-5334 (1976).
124. H. Petersen, A. Bianconi, F. C. Brown and R. Z. Bachrach, The absolute N_2 K-photoabsorption cross section up to $\hbar\omega$=450 eV, Chem. Phys. Lett. 58, 263-266 (1978).
125. J. Stöhr and R. Jaeger, Absorption-edge resonances, core-hole screening, and orientation of chemisorbed molecules: CO, NO, and N_2 on Ni(100), Phys. Rev. B

26, 4111-4131 (1982).
126. A. Bianconi, F. C. Brown and R. Z. Bachrach, (unpublished); and A. Bianconi, X-Ray Absorption Near Edge Structure (XANES) and their applications to local structure determination, in: EXAFS for inorganic systems, (C. D. Garner and S. S. Hasnain, eds.), Daresbury Report DL/SCI/R17, 13-22 (1981).
127. A. P. Hitchcock and C. E. Brion, Carbon K-shell excitation of C_2H_2, C_2H_4, C_2H_6 and C_6H_6 by 2.5 keV, J. Electron Spectrosc. & Relat. Phenom. 10, 317-330 (1977).
128. M. Dell'Ariccia, A. Gargano, C. R. Natoli and A. Bianconi, A calculation of C K-shell X-Ray Absorption Spectra of C_2H_n (n=2,4,6) oriented molecules: correlation between position of the multiple scattering resonance in the continuum and the C-C bond length, LNF Report 84/51(P).
129. S. Della Longa, M. Pompa, A. Soldatov, A. Marcelli and A. Bianconi, (unpublished).
130. C. R. Natoli, Inner Shell X-Ray Photoabsorption as a Structural and Electronic Probe of Matter, Lectures "NATO Advanced Study Institute" (1987) Vimeiro, Portugal; LNF Report 87/83 (PT); and references therein.
131. F. Sette, J. Stöhr and A. P. Hitchcock, Determination of intramolecular bond lengths in gas phase molecules from K shell shape resonances, J. Chem. Phys. 81, 4906-4914 (1984).
132. J. Stöhr, F. Sette and A. L. Johnson, Near-Edge X-Ray-Absorption Fine-Structures Studies of Chemisorbed Hydrocarbons: Bond Lengths with a Ruler, Phys. Rev. Lett. 53, 1684-1687 (1984).
133. D. Arvanitis, K. Baberschke, L. Wenzel and U. Döbler, Experimental Study of the Chemisorbed State of C_2H_2, C_2H_4 and C_2H_6 on Noble-Metal Surfaces, Phys. Rev. Lett. 57, 3175-3178 (1986).
134. D. Arvanitis, L. Wenzel and K. Baberschke, Direct Evidence of a Stretched C-C Distance for C_2H_2 and C_2H_4 on Cu(100) at 60K, Phys. Rev. Lett. 59, 2435-2438 (1987).
135. J. Stöhr, D. A. Outka, K. Baberschke, D. Arvanitis and J. A. Horsley, Identification of C-H resonances in the K-shell excitation spectra of gas-phase, chemisorbed, and polymeric hydrocarbons, Phys. Rev. B 36, 2976-2979 (1987).
136. J. Stöhr, K. Baberschke, R. Jaeger, R. Treichler and S. Brennan, Orientation of Chemisorbed Molecules from Surface-Absorption Fine-Structure Measurements: CO and NO on Ni(100), Phys. Rev. Lett. 47, 381-384 (1981).
137. J. Stöhr and D. A. Outka, Determination of molecular orientations on surfaces from the angular dependence of near-edge x-ray absorption fine-structure spectra, Phys. Rev. B 36, 7891-7905 (1987).
138. D. A. Outka, J. Stöhr, W. Jark, P. Stevens, J. Solomon and R. J. Madix, Orientation and bond length of molecular oxygen on Ag(110) and Pt(111): A near-edge x-ray-absorption fine-structure study, Phys. Rev. B 35, 4119-4122 (1987).
139. J. Stöhr, J. L. Gland, E. B. Kollin, R. J. Koestner, A. L. Johnson, E. L. Muetterties and F. Sette, Desulfurization and Structural Transformation of Thiophene on the Pt(111) Surface, Phys. Rev. Lett. 53, 2161-2164 (1984).
140. G. Tourillon, E. Dartyge, A. Fontaine, R. Garrett, M. Sagurton, P. Xu and G. P. Williams, Chemisorption geometry of poly-3-methylthiophene electrochemically deposited on Pt as observed by NEXAFS, Europhys. Lett. 4, 1391-1396 (1987).